Scintillation + Photo Detection

- Inorganic scintillators

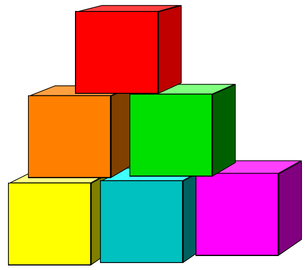

- Organic scintillator

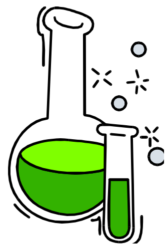

- Readout & fiber tracking

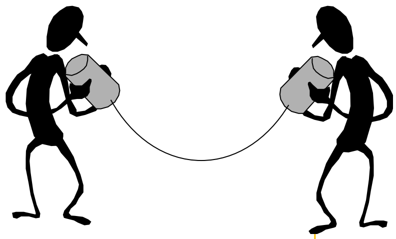

- Photo detectors

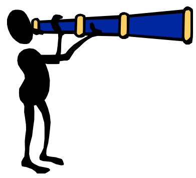

Scintillation

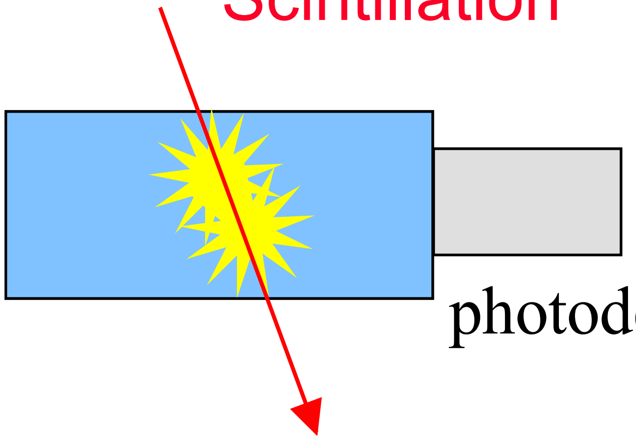

Energy deposition by ionizing particle → excited molecules → small fraction of energy released as optical photons (scintillation light or luminescense)

Scintillators multi purpose detectors

- calorimetry
- time of flight measurement
- tracking detectors (fibers)
- trigger counters
- veto counters

  …..

Two material types: Inorganic & organic scintillators

Inorganic	Organic
(generally)	
high light output but slow	lower light output but fast

3 different scintillation mechanisms:

1a. Inorganic crystalline scintillators (NaI, CsI, BaF_2...)

most common: sodium iodide with thallium trace [NaI(Tl)]

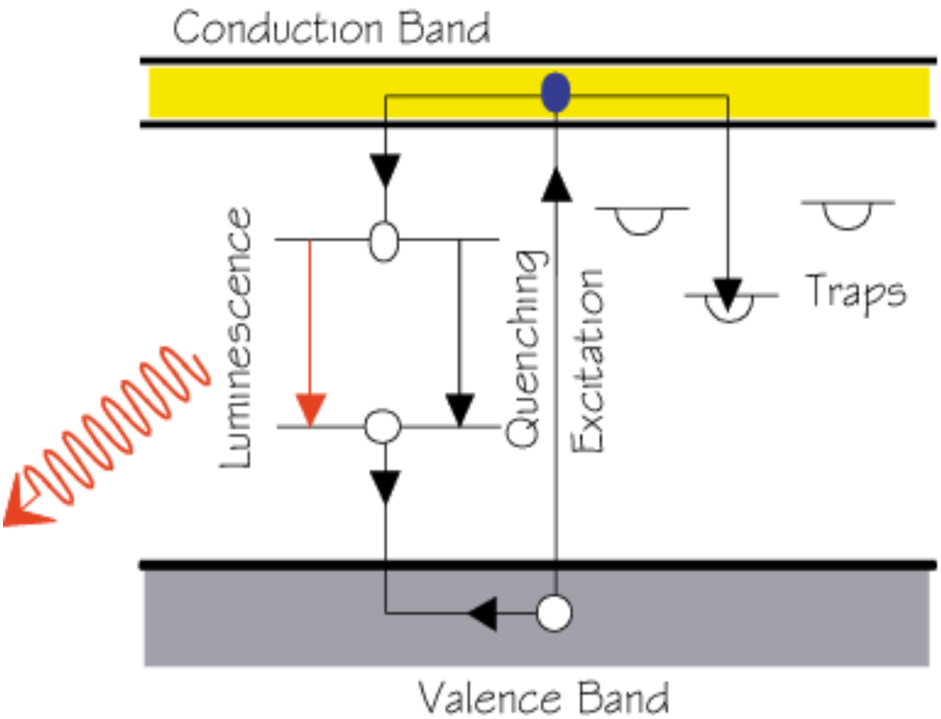

energy bands in crystals activated by impurity traces, often ≥ 2 time constants:

- fast recombination (10 ns - 1μs) from activation centers
- delayed recombination due to trapping (~100 ms)

light output of inorganic scintillators wavelength dependent

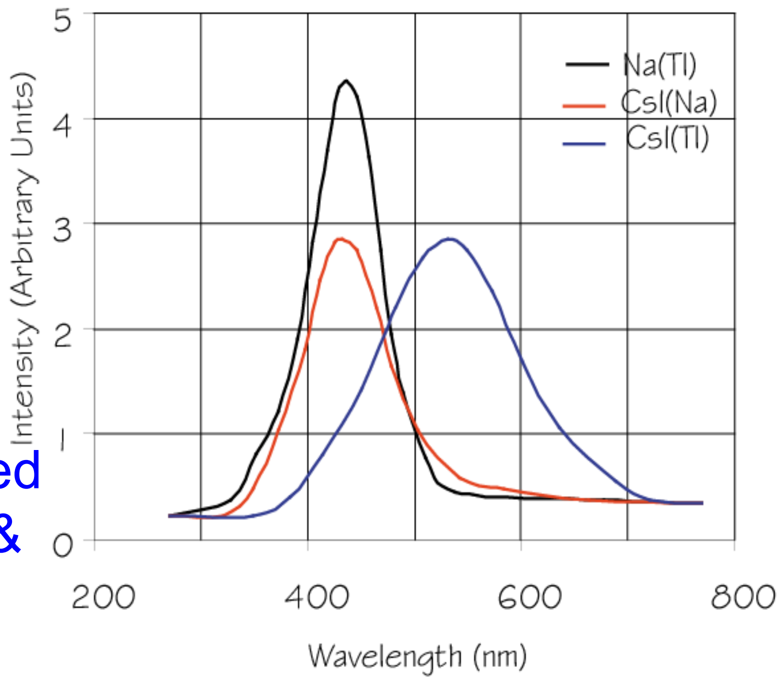

due to high density & high Z inorganic scintillators well suited for charged particle & photon detection.

Light output of inorganic crystals also shows strong temperature dependence

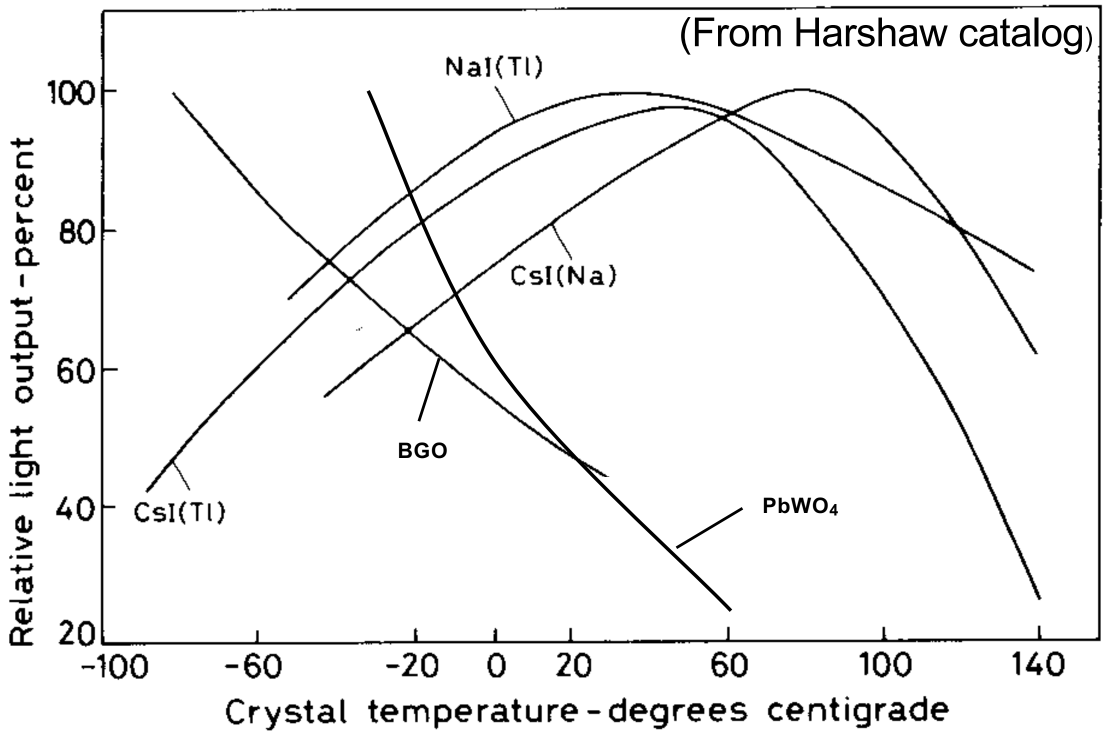

1b. Liquid noble gases (LAr, LXe, LKr)

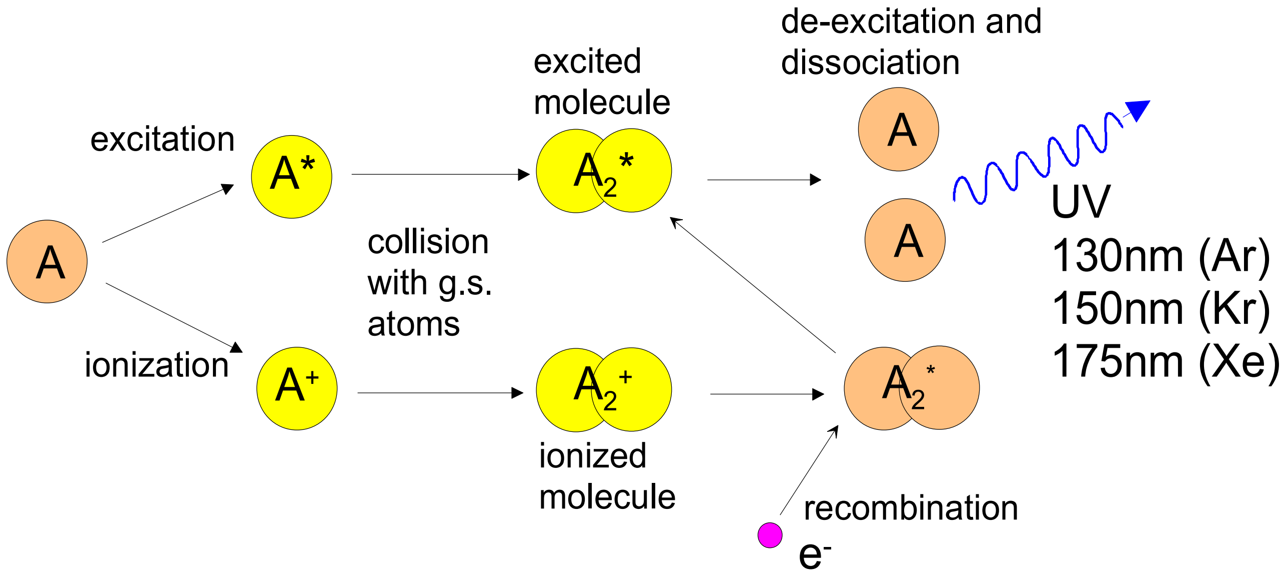

also here one finds 2 time constants: one at few ns & a second at 10 –1000 ns but both at same wavelength.

Properties of some inorganic crystal scintillators

pdg.lbl.gov   for a MIP   wavelength of maximum emission

Parameter:	ρ	MP	$X_0{}^*$	$R_M{}^*$	dE/dx^*	$\lambda_I{}^*$	τ_{decay}	λ_{max}	$n^\dagger$	Relative output‡	Hygroscopic?	$d(\mathrm{LY})/dT$
Units:	g/cm^3	°C	cm	cm	MeV/cm	cm	ns	nm				%/°C§
NaI(Tl)	3.67	651	2.59	4.13	4.8	42.9	245	410	1.85	100	yes	−0.2
BGO	7.13	1050	1.12	2.23	9.0	22.8	300	480	2.15	21	no	−0.9
BaF_2	4.89	1280	2.03	3.10	6.5	30.7	650^s	300^s	1.50	36^s	no	-1.9^s
							$<0.6^f$	220^f		4.1^f		0.1^f
CsI(Tl)	4.51	621	1.86	3.57	5.6	39.3	1220	550	1.79	165	slight	0.4
CsI(Na)	4.51	621	1.86	3.57	5.6	39.3	690	420	1.84	88	yes	0.4
CsI(pure)	4.51	621	1.86	3.57	5.6	39.3	30^s	310	1.95	3.6^s	slight	−1.4
							6^f			1.1^f		
$PbWO_4$	8.30	1123	0.89	2.00	10.1	20.7	30^s	425^s	2.20	0.3^s	no	−2.5
							10^f	420^f		0.077^f		
LSO(Ce)	7.40	2050	1.14	2.07	9.6	20.9	40	402	1.82	85	no	−0.2
PbF_2	7.77	824	0.93	2.21	9.4	21.0	-	-	-	Cherenkov	no	-
CeF_3	6.16	1460	1.70	2.41	8.42	23.2	30	340	1.62	7.3	no	0
$LaBr_3$(Ce)	5.29	783	1.88	2.85	6.90	30.4	20	356	1.9	180	yes	0.2
$CeBr_3$	5.23	722	1.96	2.97	6.65	31.5	17	371	1.9	165	yes	−0.1

sensitive to humidity?

*Numerical values calculated using formulae in this review.
†Refractive index at the wavelength of the emission maximum.
‡Relative light output measured for samples of 1.5 X_0 cube with a Tyvek paper wrapping and a full end face coupled to a photodetector. The quantum efficiencies of the photodetector are taken out.
§Variation of light yield with temperature evaluated at the room temperature.
f = fast component, s = slow component

Light yield normalized to NaI(Tl) ~ 40k photons / MeV
NB! light output dependent on light collection efficiency & quantum efficiency of photo detector (see following pages)

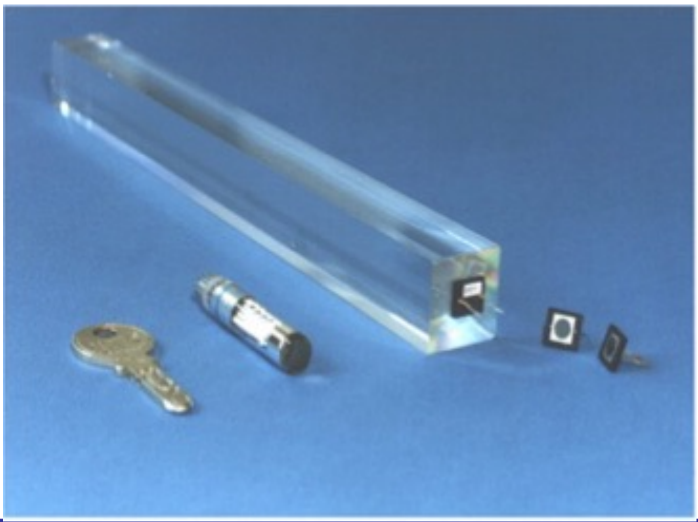

A lead tungstate ($PbWO_4$) crystal for the CMS electromagnetic calorimeter. $PbWO_4$ has fast signal, high density & good radiation tolerance at reasonable cost. Only disadvantage is relatively low light yield.

2. Organic scintillators: liquid or plastic solutions original emitted light in UV range

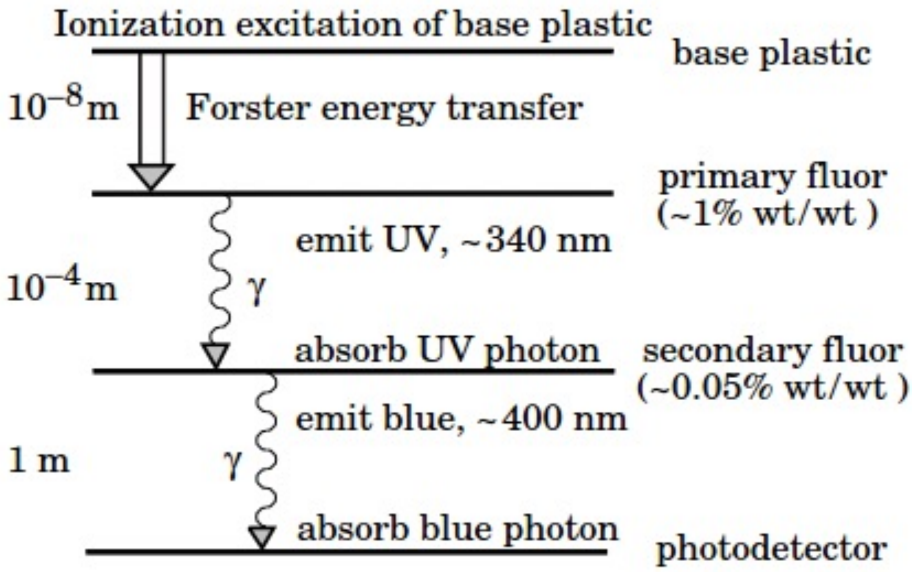

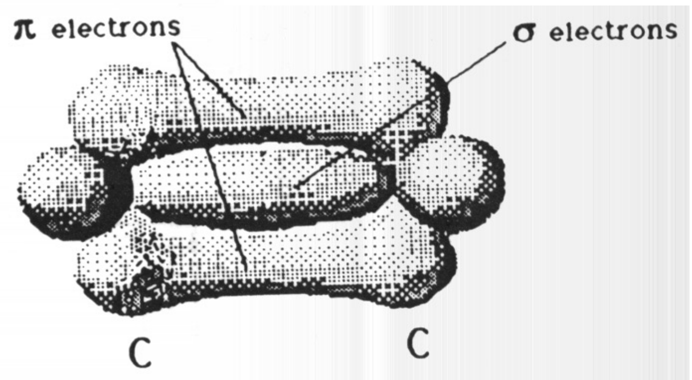

Scintillation based on the two "π" electrons of the C–C bonds in "aromatic rings" like benzene.

Normally made of plastic base/solvent & primary fluor + secondary (& tertiary) fluors as wavelength shifters.

Fast energy transfer from plastic base/solvent to fluors via resonant dipole-dipole interactions ("Förster transfer") since short distances between molecules
→ shift emission to longer wavelengths
→ longer absorption length & more efficient read-out

Organic scintillators have low Z (H,C) → low photon detection efficiency but high neutron efficiency via (n,p) reactions. Reasonable for charged particles.

Schematic representation of wave length shifting principle

(C. Zorn, Instrumentation In High Energy Physics, World Scientific,1992)

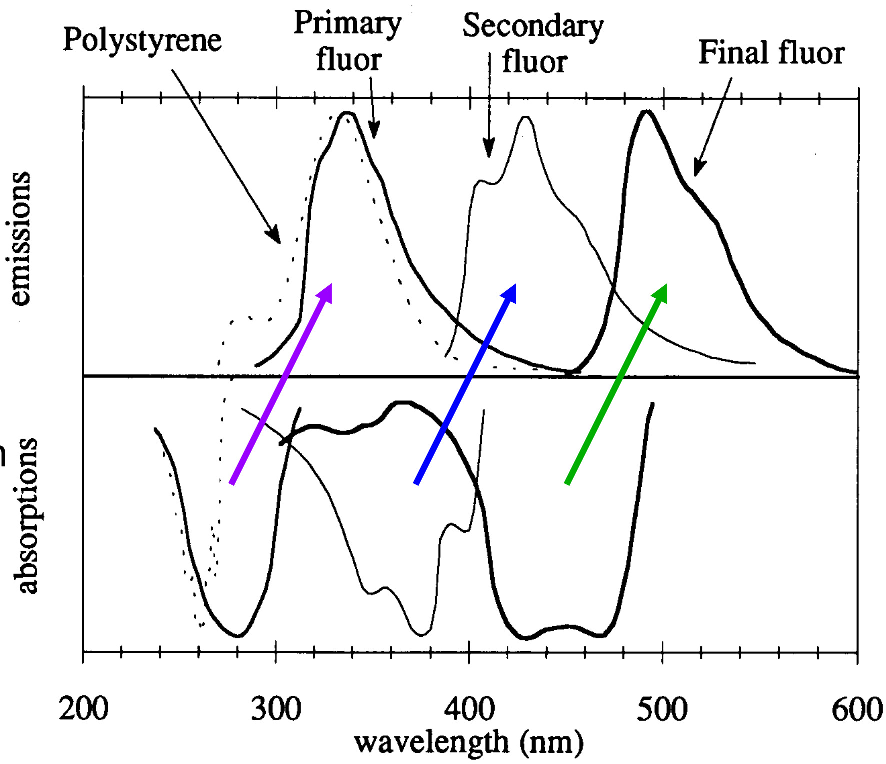

Some widely used plastic scintillators:

Scintillator material	Density [g/cm^3]	Refractive Index	Wavelength [nm] for max. emission	Decay time constant [ns]	Photons/MeV
Naphtalene	1.15	1.58	348	11	$4\cdot10^3$
Antracene	1.25	1.59	448	30	$4\cdot10^4$
p-Terphenyl	1.23	1.65	391	6-12	$1.2\cdot10^4$
NE102*	1.03	1.58	425	2.5	$2.5\cdot10^4$
NE104*	1.03	1.58	405	1.8	$2.4\cdot10^4$
NE110*	1.03	1.58	437	3.3	$2.4\cdot10^4$
NE111*	1.03	1.58	370	1.7	$2.3\cdot10^4$
BC400**	1.03	1.58	423	2.4	$2.5\cdot10^2$
BC428**	1.03	1.58	480	12.5	$2.2\cdot10^4$
BC443**	1.05	1.58	425	2.2	$2.4\cdot10^4$

* Nuclear Enterprises, U.K.
** Bicron Corporation, USA

After mixing components together plastic scintillators produced by a complex polymerization method. Plastic scintillators very easy to form any desired shape.

Scintillator readout

Readout to be adapted to geometry & emission spectrum of scintillator (need to shift wavelength?).

Geometrical adaptation:

wavelength shifter (WLS) bars

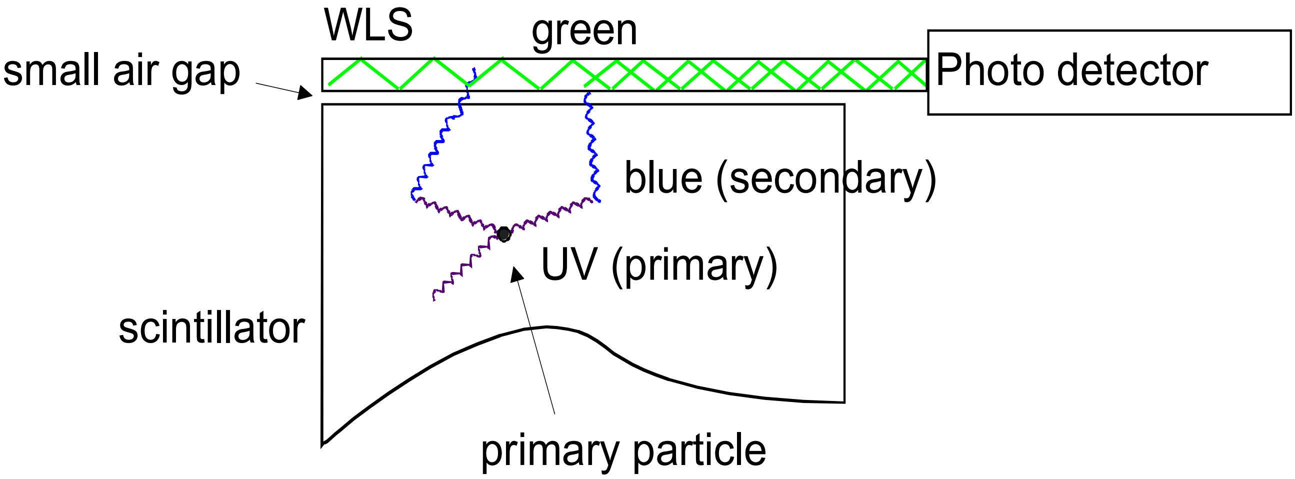

optical fibers & light guides: light transport by total internal reflection (& outer reflector for light guides)

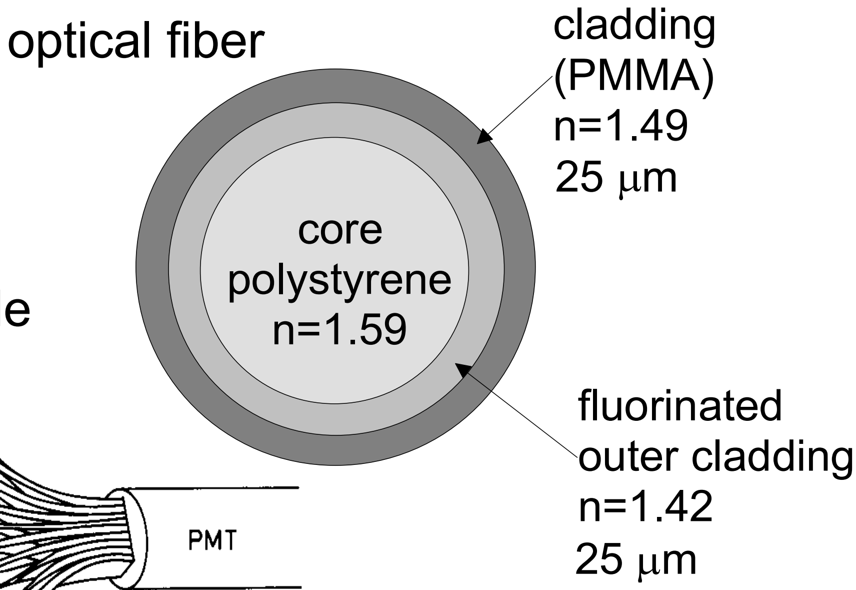

adiabatic light guide

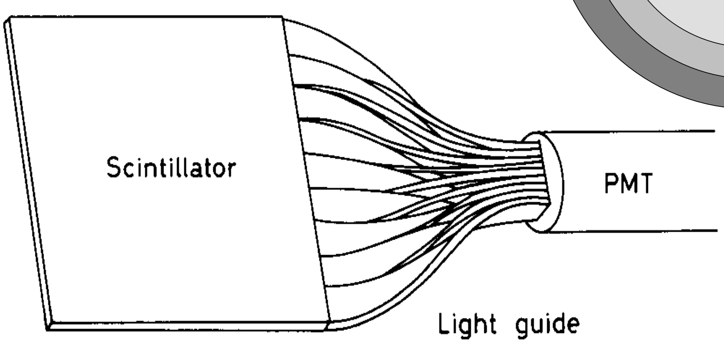

Scintillating fiber tracking

- Scintillating plastic fibers
- Capillary fibers, filled with liquid scintillator

- High geometrical flexibility & low mass
- Fine granularity & good hermeticity (="no holes")
- Fast response (ns) (if fast read out) → 1st level trigger

Hexagonal fibers with double cladding. In figure only central fiber illuminated ⇒ low cross talk !

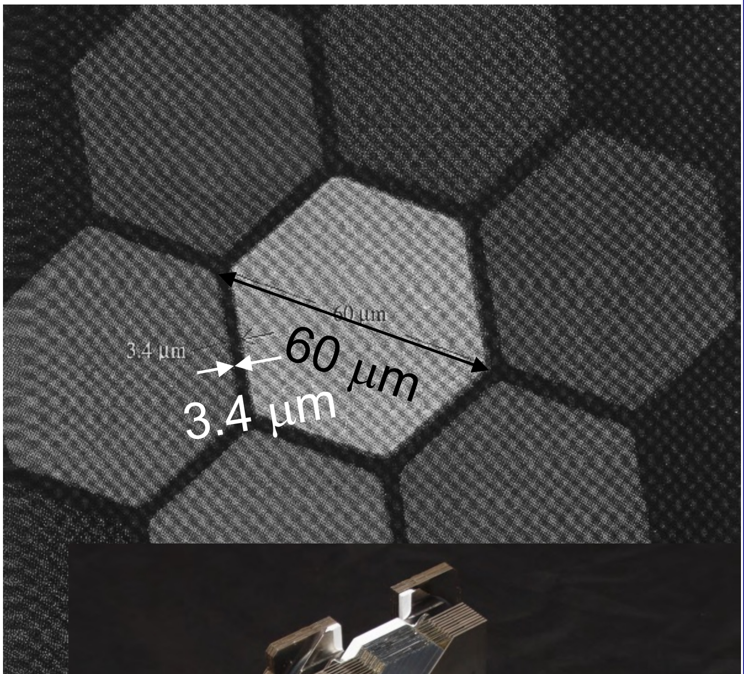

Number of photons produced by a traversing minimum ionizing particle not very high so need efficient readout. 1 mm fiber → < 2000 photons. Taking into account fiber attenuation, capturing & photo detector efficiency ~10–20 photons remain (must be careful not to loose signal).

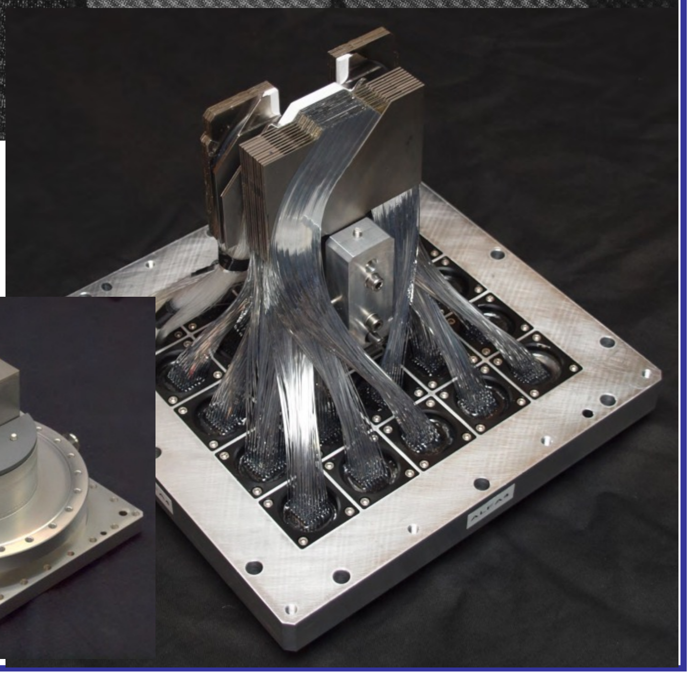

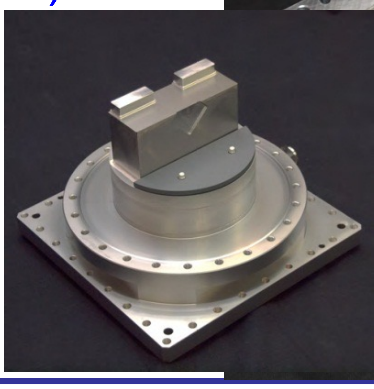

ATLAS/ALFA scintillating fiber tracker for leading proton measurement ~240m from IP using Roman Pots

purpose: convert light into detectable electronics signal
principle: Use photoelectric effect to convert photons to photo–electrons (multiplied by some mechanism)

Photoemission threshold W_{ph} of various materials

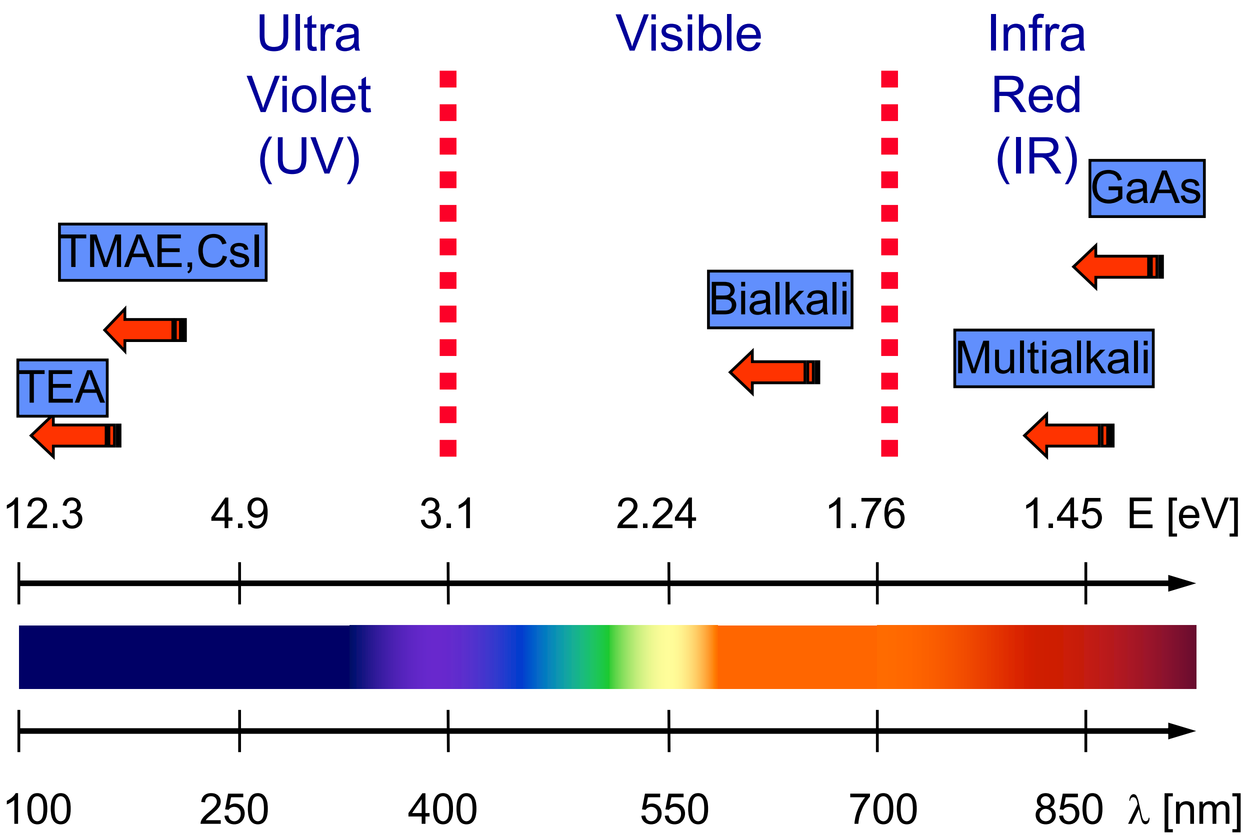

standard requirement

- high sensitivity, usually expressed as quantum efficiency $Q.E. = N_{photo\ electrons} / N_{photons}$

Main types of photo detectors

- gas based (use photosensitive additive e.g. TMAE)
- vacuum based (photosensitive photo–cathode)
- solid state detectors (e.g. GaAs)

Photo Multiplier Tube (PMT)

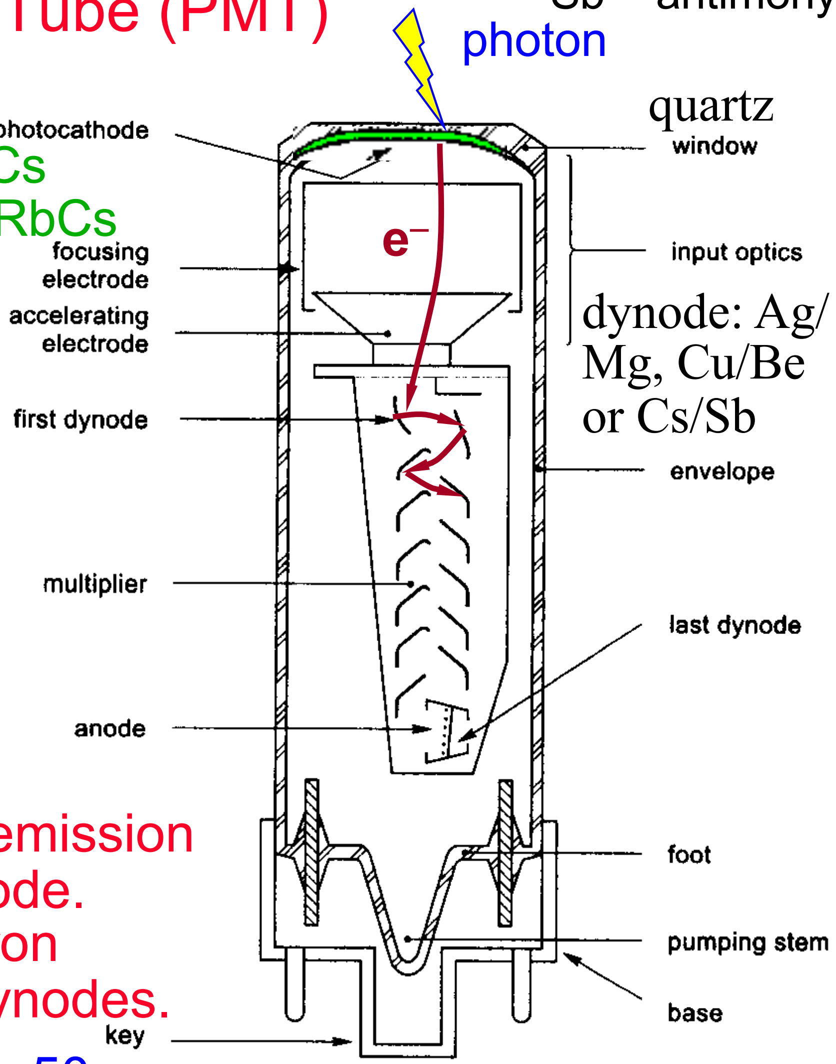

Photo–cathode:
Multialkali: $SbNa_2KCs$
Bialkali: SbKCs, SbRbCs

(Philips Photonic)

main phenomena:
- Photo-electron emission from photo-cathode.
- secondary electron emission from dynodes.

dynode gain: g = 3–50

total gain: $M = \prod_{i=1}^{N} g_i$

For example: 10 dynodes with $g = 4 \Rightarrow M = 4^{10} \approx 10^6$

PMT's very sensitive to magnetic fields, even to earth field (30-60 μT). metal shielding required.

Photoelectric effect in photo–cathode 3-step process:
- absorbed γ's give energy to e's in photo–cathode (PC)
- e's diffuse through PC, losing part of their energy
- e's reaching surface with enough energy to escape PC

ideal photo–cathode absorb all γ's & emit all created e's
emission threshold $W_{ph} > E_g$ (band gap) + E_a (electron affinity)

Quantum efficiencies of typical photo–cathodes

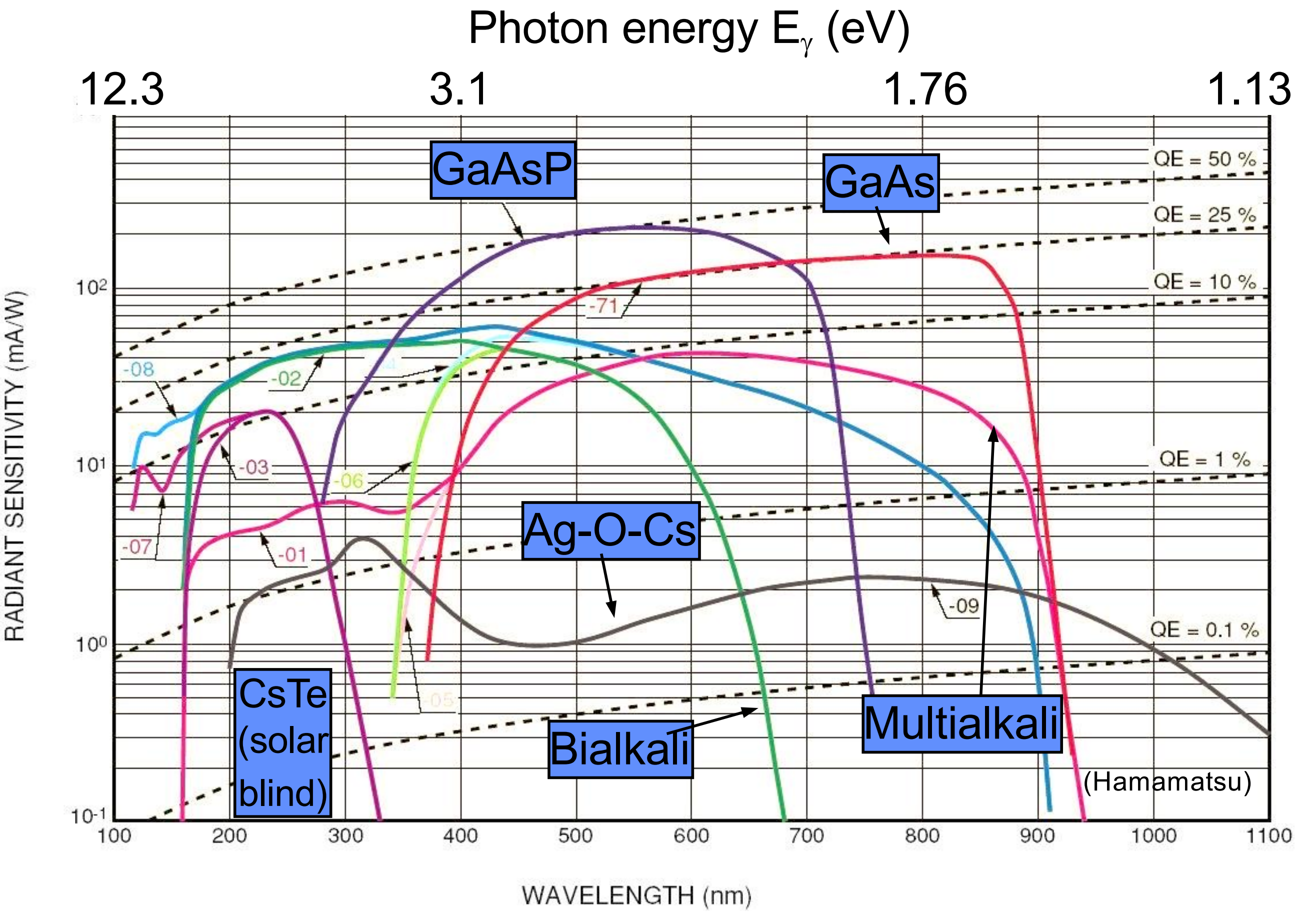

Energy resolution of PM's: determined by fluctuations of the number of secondary electrons emitted by dynodes (follows a Poisson distribution with expectation value $\bar{n}$).

Relative resolution: $\frac{\sigma_n}{\bar{n}} = \frac{\sqrt{\bar{n}}}{\bar{n}} = \frac{1}{\sqrt{\bar{n}}}$ (fluctuations at the first dynode most important!!)

Multi anode PM´s e.g Hamamatsu R5900 series

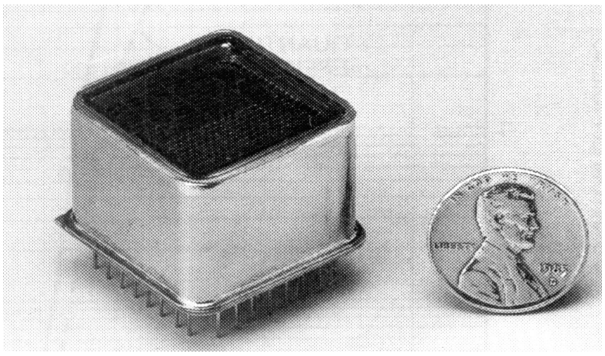

up to 8x8 channels.
size: 28x28 mm^2.
active area 18x18 mm^2 (41%).
bialkali PC: Q.E. = 20% at λ_{max} = 400 nm. Gain ≈ 10^6.

Silicon photodiodes & photomultipliers (SiPM)

- Silicon used when detecting near UV to visible light
- Silicon diode technology well advanced with high QE (better than 80 % at most sensitive wavelengths)
- Silicon devices tolerant to quite high radiation levels
- Silicon photodiodes linear over many orders of magnitude

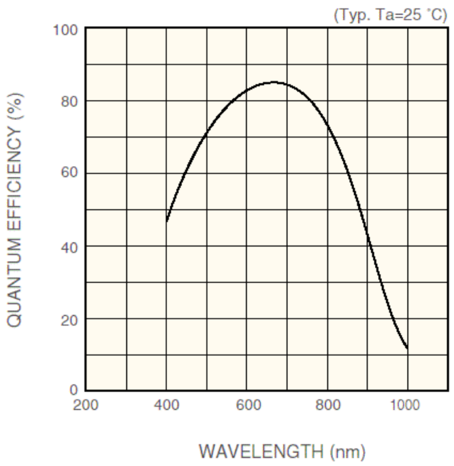

multi-pixel photon counters (MPPCs) (for new TOTEM T2) & single SiPMs

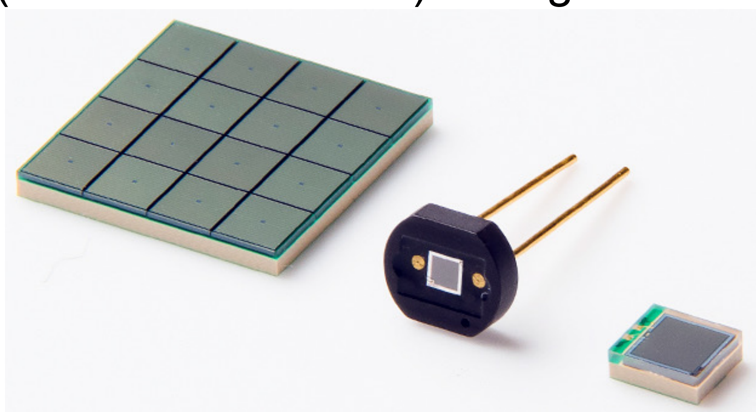

Hybrid photo diodes (HPD) – large window in wave length for photon acceptance

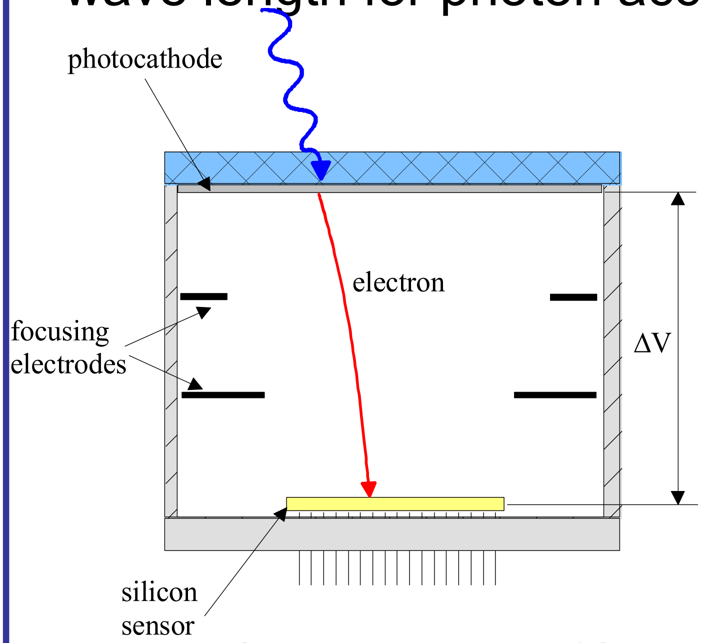

Photo–cathode like in PMT, ΔV = 10–20 kV

photo electron acceleration + silicon detector (pixels or strips)

$$G = \frac{e\Delta V}{W_{Si}} = \frac{20\ keV}{3.6\ eV} \approx 5\times10^3$$

Q.E. ≈ 10 - 30 %

can do real single photon counting !!

Avalanche photodiodes (APD)

e.g. CMS electromagnetic calorimeter

- Operated at a gain of 50
- Active area of 2x25mm²/crystal
- Q.E. ~ 80% for $PbWO_4$ emission
- High reverse bias voltage (100-200 V)
- High internal field → avalanche multiplication.
- Sub-ns response time
- Irradiation causes bulk leakage current to increase
  → electronic noise doubles after ~10 yrs - **acceptable**

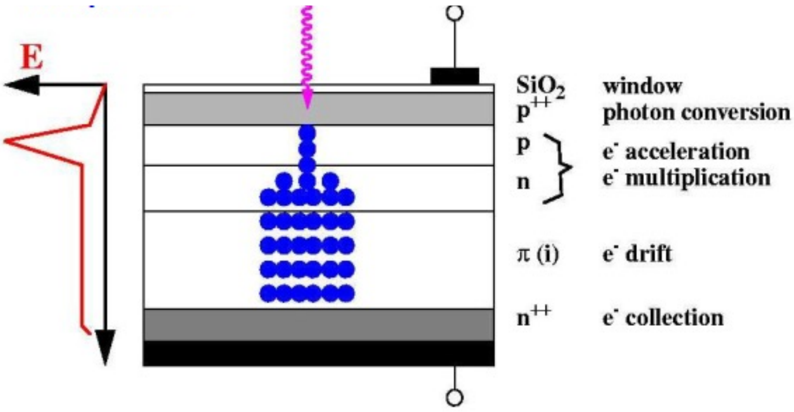

Each crystal has two 5x5 mm² APDs

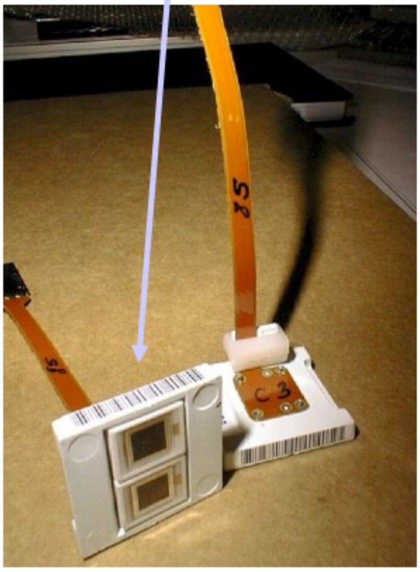

Vacuum phototriodes (VPT)

B-field orientation in end caps favourable for VPTs (tube axes $8.5° < |\theta| < 25.5°$ with respect to field

Vacuum devices offer greater radiation hardness than Si diodes

- Gain: 8-10 at B = 4T
- Active area of ~280 mm²/crystal
- Q.E. ~ 20% at 420 nm
- Insensitive to shower leakage particles
- UV glass window – less expensive than "quartz"
  - ✓ more radiation resistant than borosilicate glass
- Irradiation causes darkening of window
  → loss in response < 20% after ~10 yrs - **acceptable**

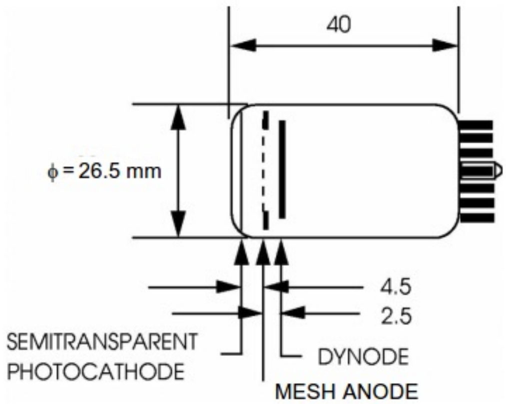

used by e.g. CMS for readout of endcap calorimeter (also already DELPHI & OPAL at LEP used same technology)

see e.g. *IEEE NS-30 No. 1 (1983) 479.*

Calorimetry

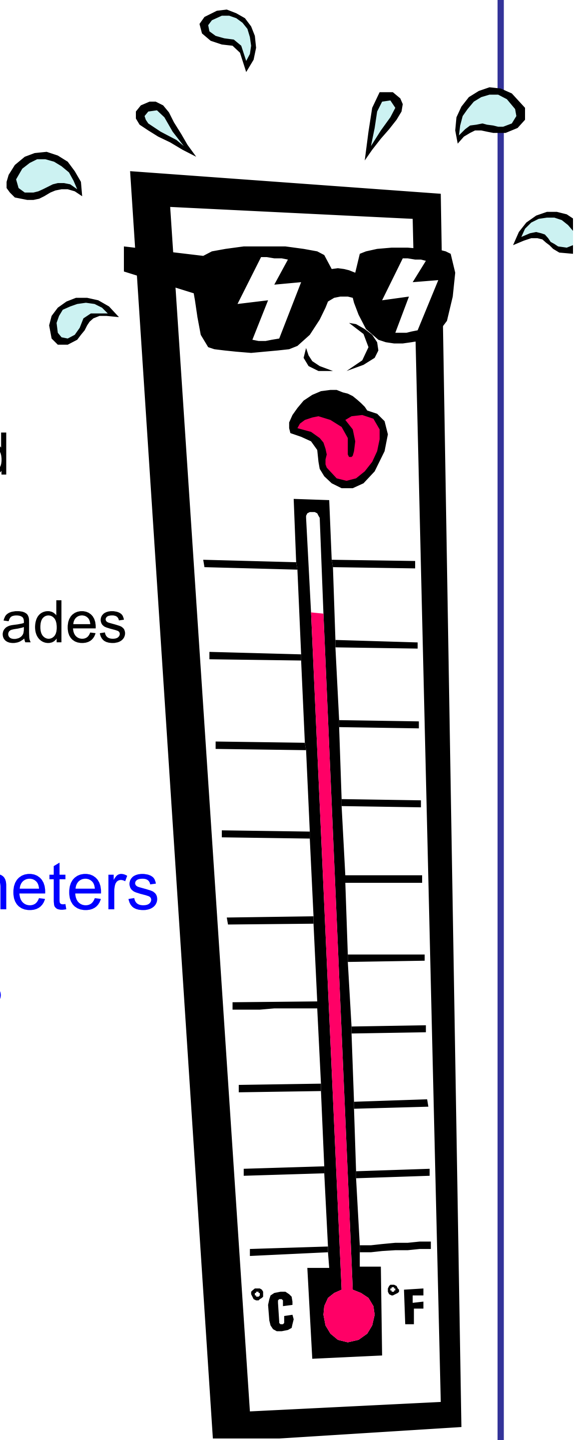

- **Basic principles**
  - Interaction of charged particles & photons
  - Electromagnetic cascades
  - Nuclear interactions
  - Hadronic cascades
- **Homogeneous calorimeters**
- **Sampling calorimeters**

- **Calorimetry:**

  Energy measurement by total absorption, combined with spatial reconstruction.

- Calorimetry a “destructive” method

- Detector response (ideally) $\propto E$

- Calorimetry works both for
  - ⇨ charged (electrons/positrons ($e^{\pm}$) & charged hadrons)
  - ⇨ neutral particles (neutral hadrons, photons (γ))

calorimetry: ”only” measurement of neutral particles

- Basic mechanism: formation of
  - ⇨ electromagnetic showers ($e^{\pm}$, γ & π^0’s)
  - ⇨ hadronic showers (charged & neutral hadrons)

- In the end, all energy converted into ionization or excitation of detector material.

- An electromagnetic part to measure $e^{\pm}$, γ & π^0’s & a hadronic part to measure all other particles

NB! π^0’s predominantly decay instantaneously to 2 γ‘s

Energy loss by Bremsstrahlung

Emission of real photons by a charged particle accelerated in the Coulomb field of the absorber nuclei

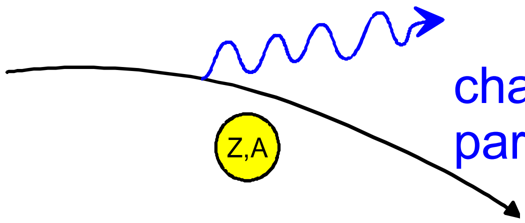

$$\frac{dE}{dx} \approx -\frac{4\alpha^3(\hbar c)^2}{\left(m_{\text{particle}}c^2\right)^2}\frac{Z^2}{A}\,N_A\,E\,z_{\text{particle}}^2\ln\left(\frac{183}{Z^{1/3}}\right)$$

Since $\propto\ m_{\text{particle}}^{-2}$, effectively plays only a role for $e^{\pm}$'s & ultrarelativistic μ's (>1 TeV)

For electrons:

$$\frac{dE}{dx} \approx -4\,\alpha\,N_A\frac{Z^2}{A}\,r_e^2\,E\ln\left(\frac{183}{Z^{1/3}}\right) \qquad r_e = \frac{\alpha\,\hbar c}{m_e c^2}$$

$$\boxed{\frac{dE}{dx} \equiv -\frac{E}{X_0}} \qquad NB!\ \left.\frac{dE}{dx}\right|_{Ioniz} \propto -Z\ln E$$

$$X_0 \approx \frac{A}{4\,\alpha\,N_A\,Z^2\,r_e^2\ln(183/Z^{1/3})}$$ radiation length

Radiation length ≡ average distance electron travels before loosing 1/e of its energy due to bremsstrahlung

Taking also into account interactions with the atomic electrons ($\propto$ Z)

$$X_0 \approx \frac{716.4\,A\ \ [\text{g/cm}^2]}{Z(Z+1)\ln\left(287/\sqrt{Z}\right)}$$

Radiation length of material defined for electrons!

For a compound: $$\frac{1}{X_0} = \sum_{j=1}^{N} \frac{w_j}{X_0^j}$$

w_j: mass fraction of components

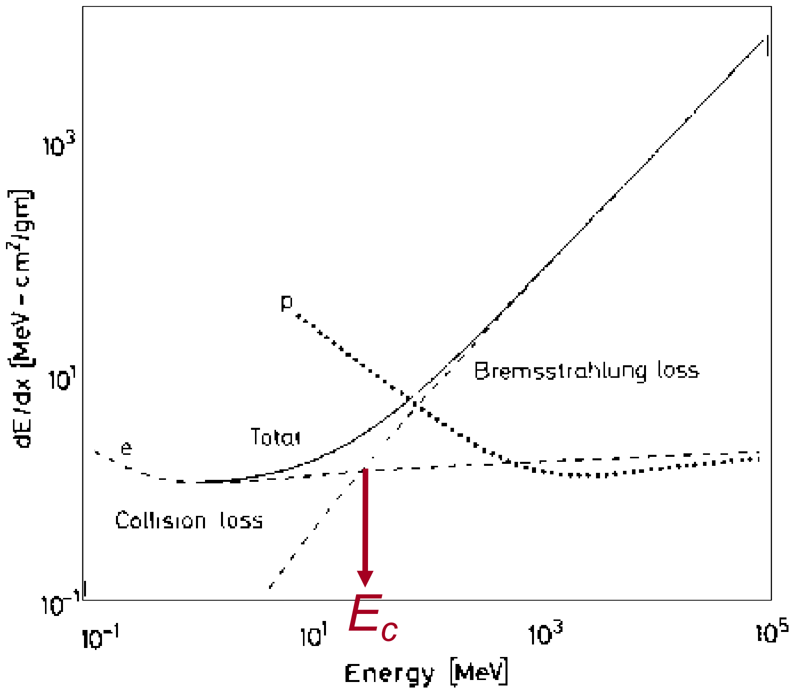

energy loss (bremsstrahlung + ionization) of electrons & protons in copper

Critical energy E_c: $$\left.\frac{dE}{dx}(E_c)\right|_{Brems} = \left.\frac{dE}{dx}(E_c)\right|_{Ioniz}$$

For electrons one finds approximately:

$$E_c^{\text{solid+liquids}} \approx \frac{610\ MeV}{Z+1.24} \qquad E_c^{\text{gas}} \approx \frac{710\ MeV}{Z+0.92}$$

For example $E_c(e)$ in Fe (Z = 26) = 22.4 MeV

For muons:

$$E_c(\mu) \approx E_c(e)\left(\frac{m_\mu}{m_e}\right)^2$$

$E_c(\mu)$ in Fe (Z = 26) ≈ 1 TeV

bremsstrahlung need only be taken into account for $e^\pm$!

Interaction of photons

To be detected, a photon must create charged particles and/or transfer energy to charged particles (note photon interaction with matter fundamentally different w.r.t. charged particles since photons either absorbed or scattered at large angle)

3 mechanisms: photo-electric effect, Compton scattering & pair production

- Photo-electric effect:

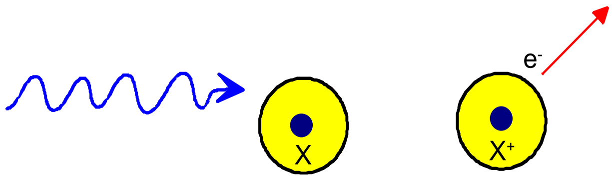

$$\gamma + \text{atom} \rightarrow \text{atom}^{+} + e^{-}$$

Only possible in close vincinity of a third collision partner (the nucleus) → photo-electric effect re-leases mainly electrons from the K–shell (≈ 80 %).

$$\sigma_{photo} \approx \frac{16}{3}\sqrt{2}\,\pi\, r_e^2\, \alpha^4\, Z^5\, \varepsilon^{-3.5} \qquad \varepsilon \equiv \frac{E_\gamma}{m_e c^2}$$

cross section shows strong modulation when $E_\gamma \sim E_{\text{ionization}}^{\text{shell}}$

At high energies ($\varepsilon \gg 1$)

$$\sigma_{photo} \approx 4\,\pi\, r_e^2\, \alpha^4\, Z^5\, \varepsilon^{-1} \qquad \boxed{\sigma_{photo} \propto Z^5}$$

• Compton scattering:

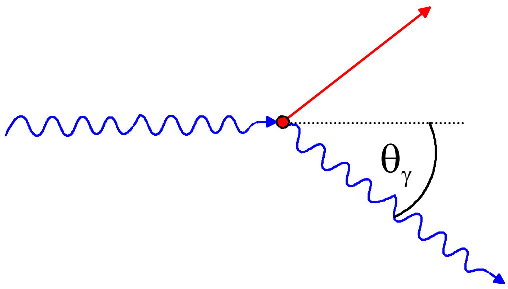

$$\gamma + e \rightarrow \gamma' + e'$$

$$E'_\gamma = E_\gamma \frac{1}{1+\varepsilon(1-\cos\theta_\gamma)}$$

Assume electron as quasi-free

cross section: Klein-Nishina formula, at high energies:

$$\sigma^e_{Compton} \approx \pi r_e^2 (0.5 + \ln 2\varepsilon)/\varepsilon \qquad \boxed{\sigma_{Compton} \propto Z}$$

atomic Compton cross-section: $\sigma^{atomic}_{Compton} \approx Z\,\sigma^e_{Compton}$

• Pair production

$$\gamma + nucleus \rightarrow e^+ e^- + nucleus$$

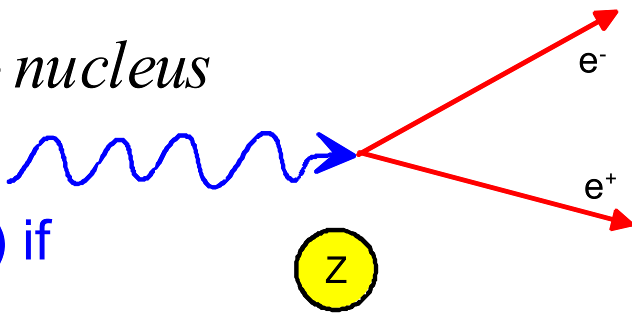

Only possible in Coulomb field of a nucleus (or an e⁻) if

$$E_\gamma \geq 2m_e c^2 \Rightarrow \varepsilon \geq 2$$

cross section (high energy approximation)

$$\sigma_{pair} \approx 4\alpha r_e^2 Z^2 \left(\frac{7}{9}\ln\frac{183}{Z^{\frac{1}{3}}}\right)$$

independent of energy !

$$\boxed{\sigma_{pair} \propto Z^2}$$

$$\approx \frac{7}{9}\frac{A}{N_A}\frac{1}{X_0} \Rightarrow \lambda_{pair} = \frac{9}{7}X_0$$

At high energies energy shared more symmetrically between e^+ & e^-

the **interaction length** for high energy photons

(Grupen)

Dominating effect in each region of atom number Z of absorber material – photon energy

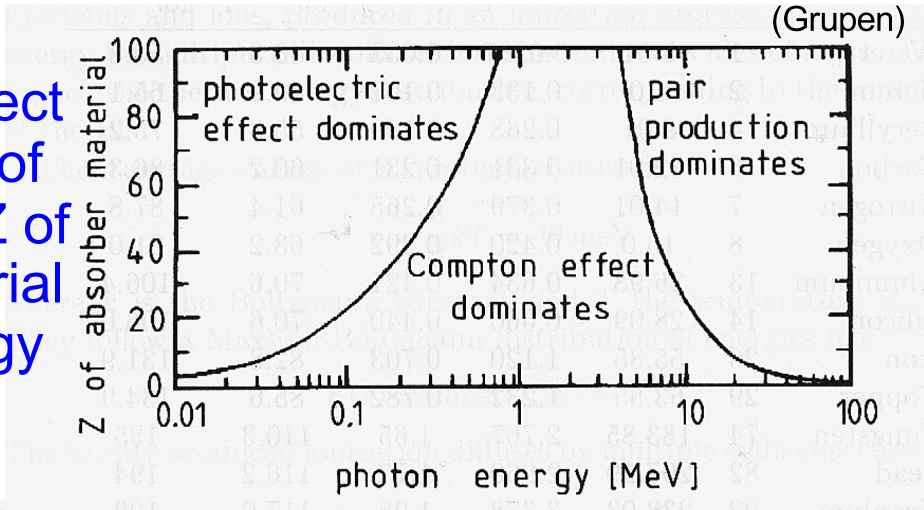

(Kleinknecht)

Photo-electric effect

Pair production

Compton scattering

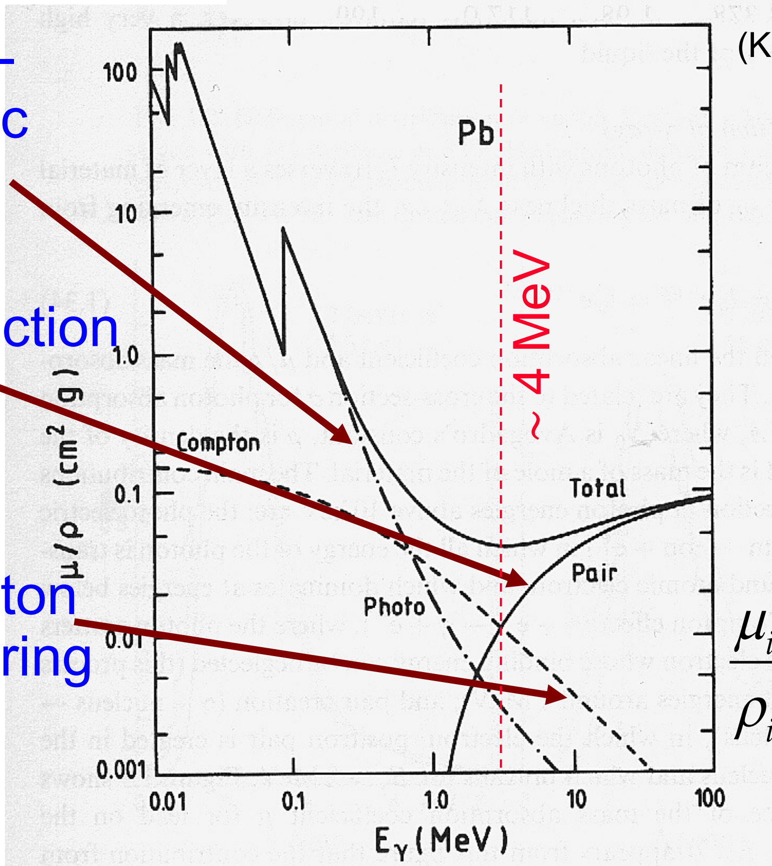

μ: linear absorption coefficient

μ/ρ: mass attenuation coefficient

$$\frac{\mu_i}{\rho_i} = \frac{N_A}{A}\sigma_i \left[cm^2/g\right]$$

In summary for photon interactions with matter: (to describe statistical process of photon attenuation):

$$I(X \text{ or } x) = I_0 e^{-\mu x} = I_0 e^{-(\mu/\rho)X} \qquad X = \rho x$$

$$\mu = \mu_{Photo} + \mu_{Compton} + \mu_{Pair} + \ldots$$

Reminder: basic electromagnetic interactions

e^+ / e^-

NB! for $e^{\pm}$ energy loss

- Ionisation

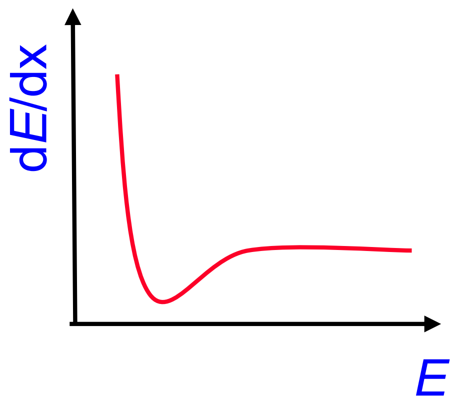

- Bremsstrahlung

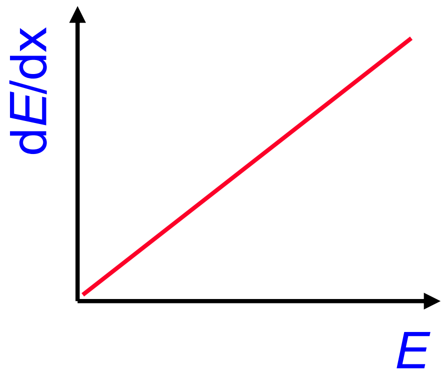

γ

NB! for γ interaction probability

- Photoelectric effect

- Compton effect

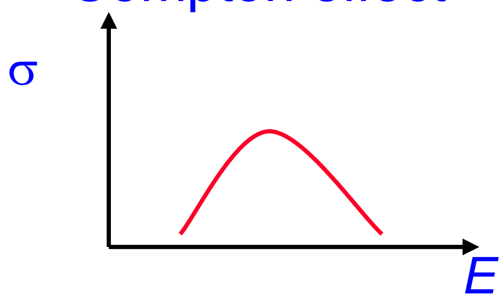

- Pair production

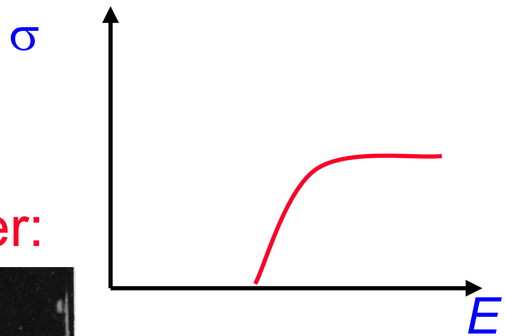

A real electromagnetic shower:

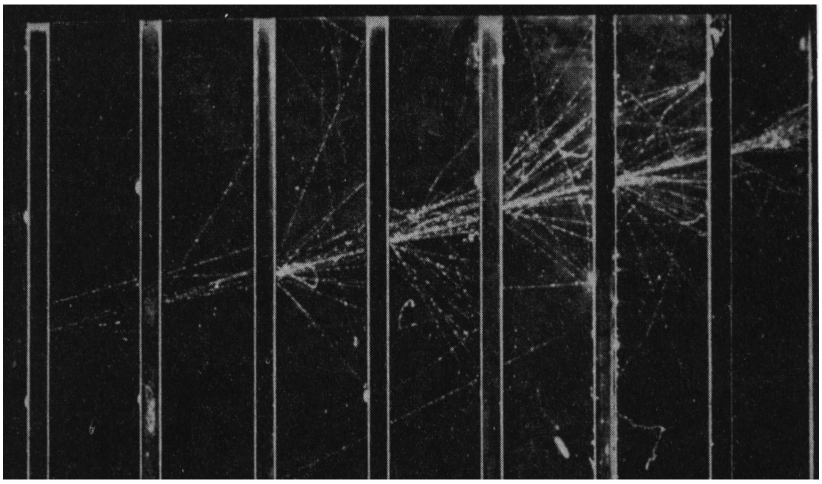

Electron shower in a cloud chamber with lead absorbers

Simple qualitative model t = # of X_0 or λ_{pair}

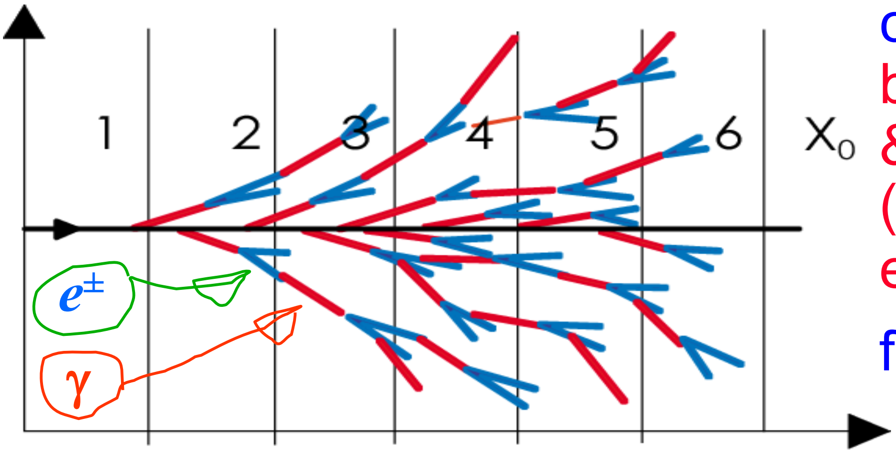

consider only bremsstrahlung & pair production (OK for high energy $e^{\pm}/\gamma$).

for simplicity: $X_0 \approx \lambda_{pair}$ & e ≈ 2

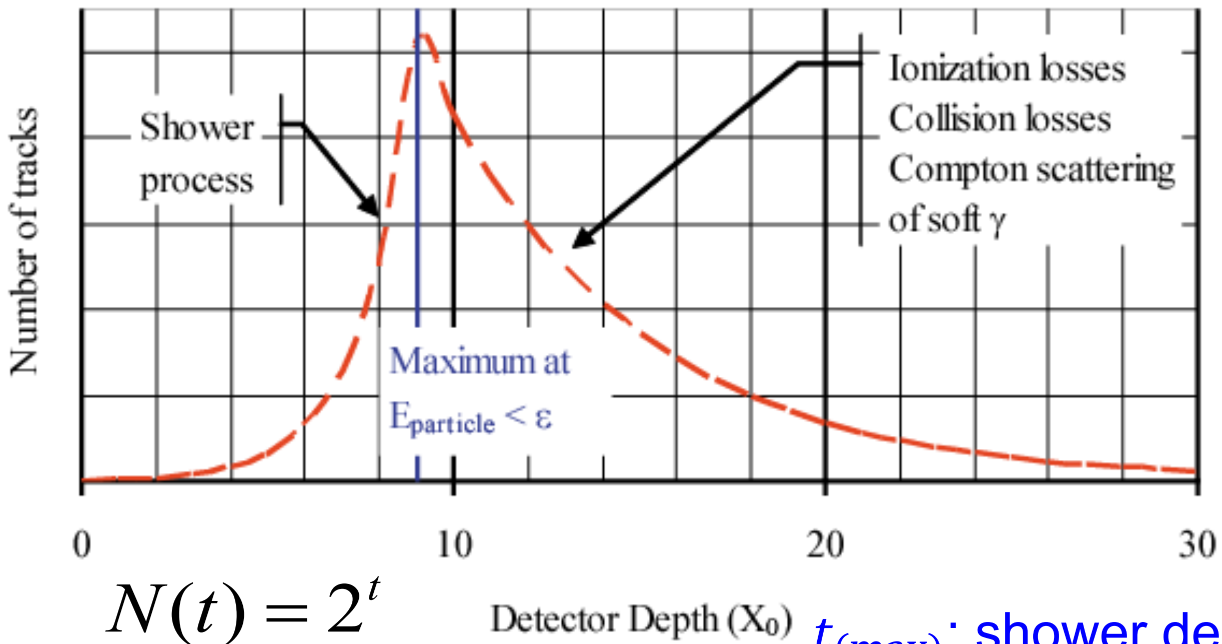

$$N(t) = 2^t$$

$$E_{particle} = E_0 \cdot 2^{-t}$$

process ends when $E_{particle} < E_c$

$t_{(max)}$: shower depth in radiation lengths (at maximal number of shower particles)

$$t_{max}^{em} = \frac{\ln E_0/E_c}{\ln 2} \qquad N^{total} = \sum_{t=0}^{t_{max}^{em}} 2^t = 2^{(t_{max}^{em}+1)} - 1 \approx 2\frac{E_0}{E_c}$$

after $t = t_{max}^{em}$ dominating processes ionization, excitation, Compton scattering & photo-electric effect → absorption.

Longitudinal shower development: $\dfrac{dE}{dt} \propto E_0 (t^{em})^{\alpha} e^{-bt}$

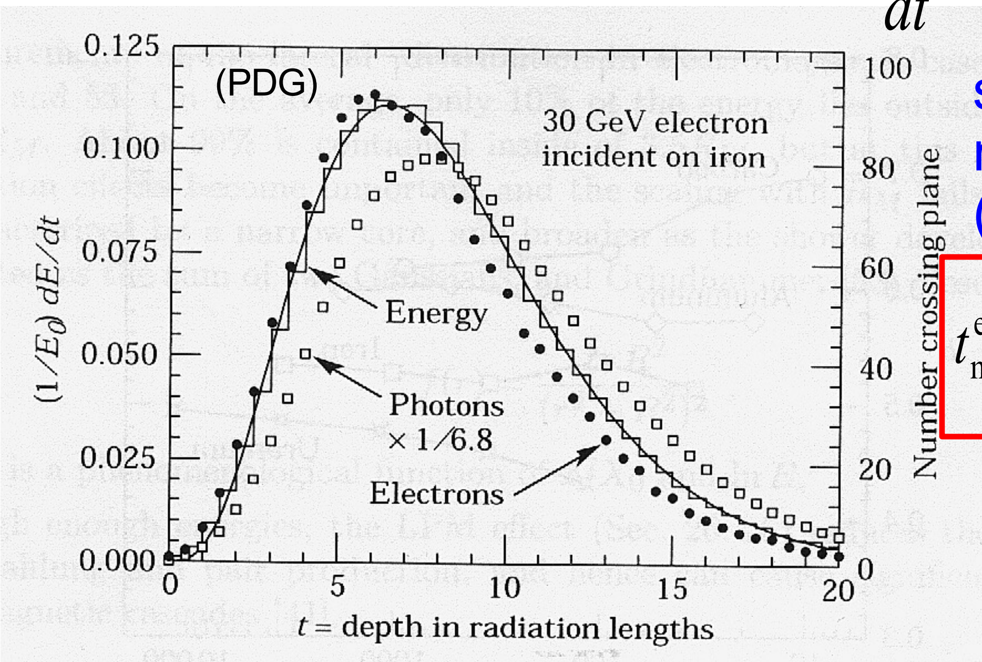

shower maximum (in reality) at

$$\boxed{t_{\max}^{em} = \ln \frac{E_0}{E_c} + C_j}$$

(C_e = –0.5; C_γ = +0.5)

98% energy containment: $t_{98\,\%} \approx 2.5 t_{\max}$

calorimetry depth should grow logarithmically with E_0

Transverse development of electromagnetic shower (mainly caused by multiple scattering of electrons & positrons with detector material): cone containing 90 (95) % of shower energy has a radius of 1(2) × R_M

$$R_M = \frac{21\ \text{MeV}}{E_c} X_0 \ \ [cm]$$

Molière radius

Example: 60 GeV electron in lead glass, E_c = 11.8 MeV → $t_{\max}^{em} \approx 8.0$, $t_{98\,\%}^{em} \approx 20.0$; $X_0 \approx 2$ cm, $R_M \approx 3.6$ cm

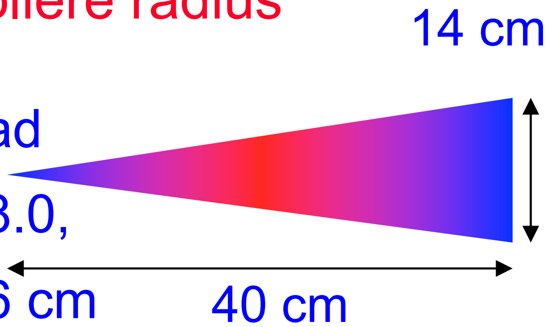

- Energy resolution of a calorimeter (intrinsic limit)

$$N^{tot} \propto \frac{E_0}{E_c}$$ total number of track segments

$$\frac{\sigma(E)}{E} \propto \frac{\sigma(N)}{N} \propto \frac{1}{\sqrt{N}} \propto \frac{1}{\sqrt{E_0}}$$ holds also for hadron calorimeters

also spatial and angular resolution scale like $1/\sqrt{E_0}$

calorimeters relative energy resolution improves with E_0 !!

More general:

$$\frac{\sigma(E)}{E} = \frac{a}{\sqrt{E}} \oplus b \oplus \frac{c}{E}$$

stochastic term

depends on the number of created secondary track segments

constant term

inhomogenities, instabilities in time, bad cell intercalibration, shower leakage

quality factor !!

noise term

electronic noise, radioactivity, pile up

Neutrinos interact only weakly → tiny cross-sections
For their detection, rely mostly on charged particles.
Possible detection reactions:

- $\nu_\ell + n/p \to \ell^\pm + p/n, \quad \ell = e, \mu, \tau$

Cross-section for reaction $\nu_e + n \to e^- + p$: O(10^{-43}) cm^2 ≈ 0.1 ab (per nucleon) for $E_\nu \approx$ few MeV.

Detection efficiency: $\varepsilon_{\mathrm{det}} = \sigma \cdot N = \sigma \cdot \rho \frac{N_A}{A} d$

1 m Iron: $\varepsilon_{\mathrm{det}} \approx 5 \cdot 10^{-17}$

Neutrino detection requires very (!!) big detectors ("light year size") or big & massive detectors (ktons) + very high neutrino fluxes ("long beam line experiments").
Event rates typically low (between O(1) and O(100))
e.g. SN1987a (supernova) detected by the Kamiokande II experiment with a handful (12) events.

In collider experiments fully hermetic detectors allow to detect neutrinos indirectly:

- sum up all visible energy & momentum.
- attribute missing (transverse) energy & momentum to neutrino.

example: For $W^\pm \to \mu^\pm + \nu_\mu$, reconstruct transverse mass:

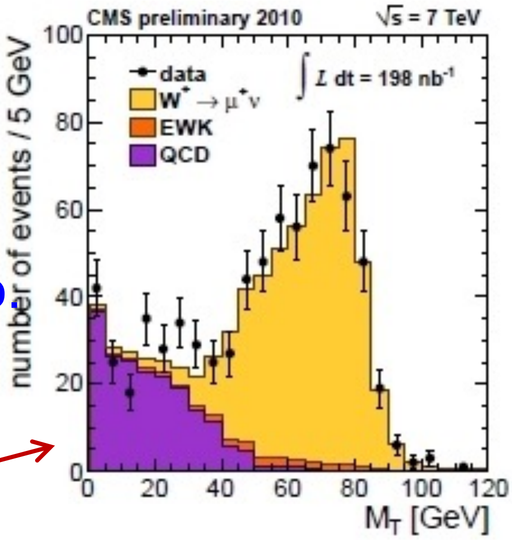

$$M_T = \sqrt{2E_T^\mu E_T^\nu \cdot [1 - \cos\Delta\phi(\mu,\nu)]}$$

Nuclear Interactions

Interaction of energetic hadrons (charged & neutral) determined by inelastic (& elastic) nuclear processes.

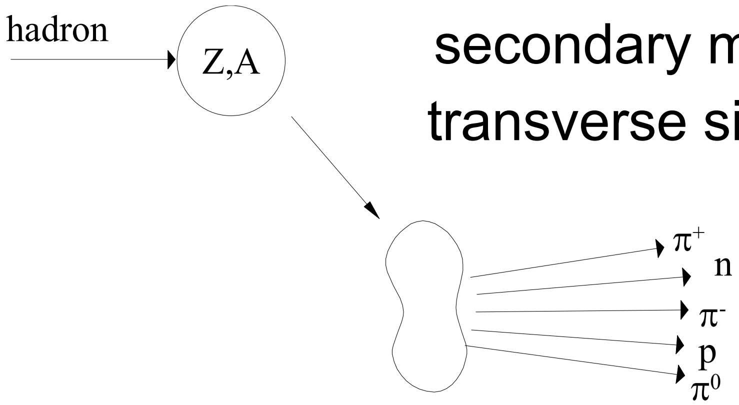

secondary multiplicity $\propto lnE$

transverse size: $\langle p_T \rangle_{\rm had} \approx$ 0.4 GeV

Elastic: no secondary particle production, only change of direction, like with multiple scattering

Inelastic: excitation & finally breakup of nucleus $\rightarrow$ nuclear fragments + secondary particle production.

For high energies (> 1 GeV) the cross-sections depend only marginally on the energy & on the type of the incident particle (p, π, K…).

$$\sigma_{\rm inel} \approx \sigma_0 \cdot A^{0.7} \qquad \sigma_0 \approx 35 \text{ mb}$$

In analogy to radiation length X_0 a hadronic interaction length can be defined (inelastic only)

$$\lambda_I = A[\mathrm{g/mol}]/(N_A \sigma_{\rm inel}) \ \propto \ A^{0.3}$$

as well a hadronic collision length (inelastic + elastic)

$$\lambda_c = A[\mathrm{g/mol}]/(N_A \sigma_{\rm tot}) \ \propto \ A^{1/3} \qquad \lambda_c < \lambda_I$$

Material	Z	A	ρ [g/cm^3]	X_0 [g/cm^2]	λ_I [g/cm^2]
Hydrogen (gas)	1	1.01	0.0899 (g/l)	63	50.8
Helium (gas)	2	4.00	0.1786 (g/l)	94	65.1
Beryllium	4	9.01	1.848	65.19	75.2
Carbon	6	12.01	2.265	43	86.3
Nitrogen (gas)	7	14.01	1.25 (g/l)	38	87.8
Oxygen (gas)	8	16.00	1.428 (g/l)	34	91.0
Aluminium	13	26.98	2.7	24	106.4
Silicon	14	28.09	2.33	22	106.0
Iron	26	55.85	7.87	13.9	131.9
Copper	29	63.55	8.96	12.9	134.9
Tungsten	74	183.85	19.3	6.8	185.0
Lead	82	207.19	11.35	6.4	194.0
Uranium	92	238.03	18.95	6.0	199.0

For Z ≥ 4: $\lambda_I > X_0$

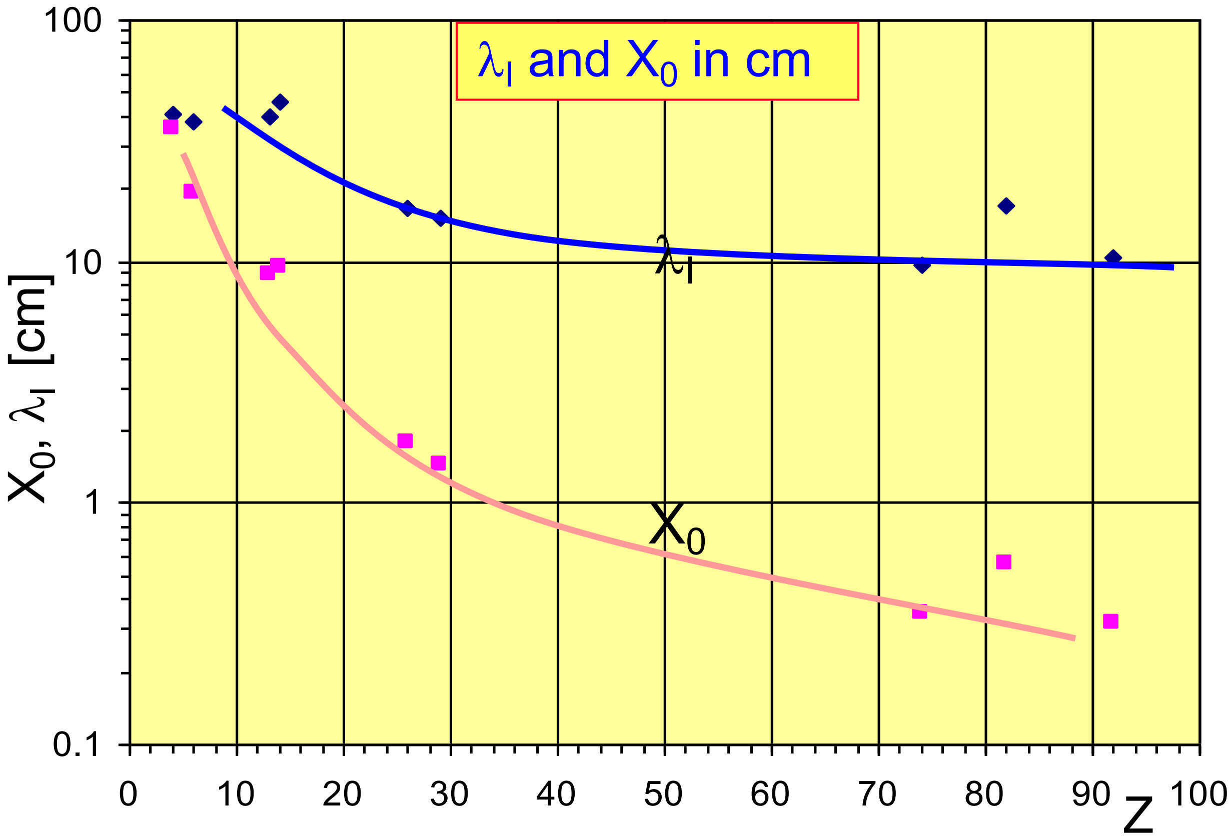

Hadronic cascades (showers)

Various processes involved → much more complex than electromagnetic cascades.

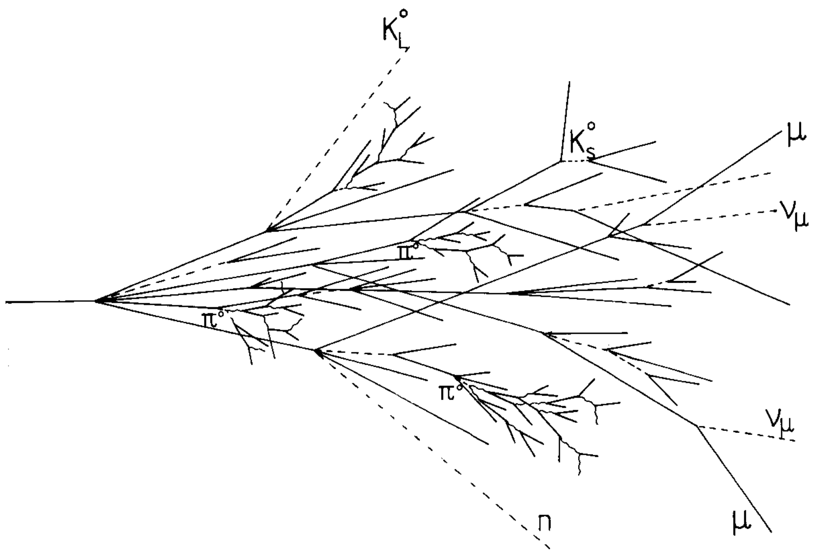

(Grupen)

hadronic + electromagnetic component

charged hadrons: $\pi^{\pm}$ (pions), $p^{\pm}$ (protons) & $K^{\pm}$ (kaons)
neutral hadrons: n (neutrons), K_S^0 & K_L^0 (neutral kaons)
→ visible energy

neutral pions (→ 2γ), electrons, γ's → electromagnetic cascade
→ visible energy

part of shower energy of lost due to ν (neutrinos), μ (muons) …

large energy fluctuations → limited energy resolution longitudinal shower development

$$t_{\max}^{\text{had}}(\lambda_I) \approx 0.2 \cdot \ln E\,[\text{GeV}] + 0.7$$
$$t_{95\%}^{\text{had}}[\text{in cm}] \approx a \cdot \ln E[\text{GeV}] + b$$

for Fe: a = 9.4, b = 39
so for E = 100 GeV
$\rightarrow t_{95\%}^{\text{had}} \approx$ 80 cm

Laterally shower consists of core + halo. 95% containment in a cylinder of radius λ_I.

Fe: λ_I = 16.7 cm

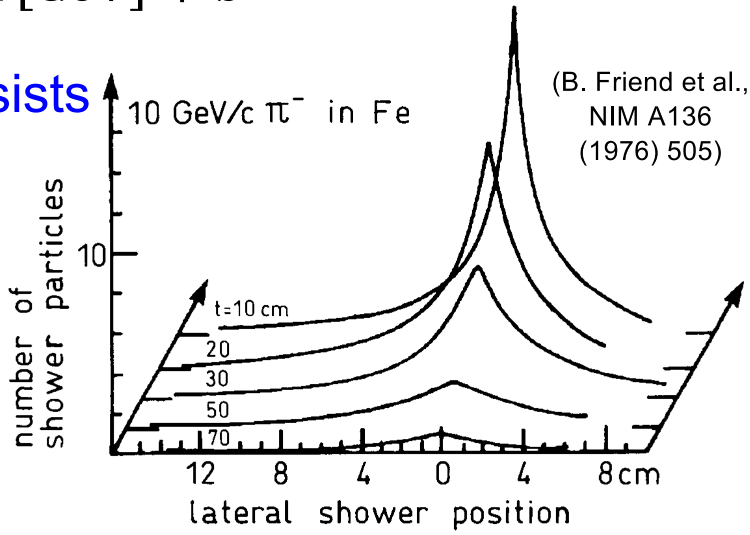

(B. Friend et al., NIM A136 (1976) 505)

Hadronic showers are much longer and broader than electromagnetic ones!

Material in front of calorimeter

Showers typically start in 'dead' material in front of calorimeter (other detectors, solenoid, support structure)

Install a highly segmented pre-shower detector in front of calorimeter

- recover lost energy
- improved background rejection due to better spatial resolution
- improve angular resolution

OPAL end cap pre-shower + calorimeter

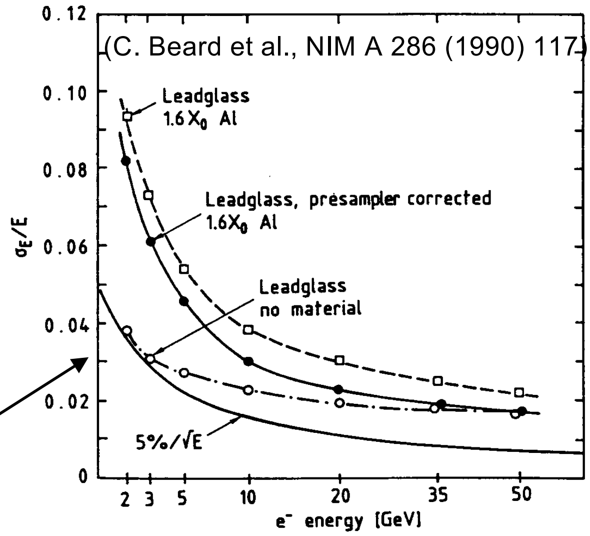

Calorimeter types

- Homogeneous calorimeters:
  - ⇨ detector = absorber
  - ⇨ good energy resolution
  - ⇨ limited spatial resolution (particularly in longitudinal direction)
  - ⇨ usually more expensive
  - ⇨ mainly used for electromagnetic calorimetry
- Sampling calorimeters:
  - ⇨ detectors & absorber separated → only fraction of the energy measured.
  - ⇨ limited energy resolution
  - ⇨ good spatial resolution
  - ⇨ used both for electromagnetic & hadronic calorimetry

Homogeneous calorimeters

two main types: scintillator crystals or “glass” blocks (that exploit Cerenkov radiation for energy measurement).
→ created photons counted using photo detectors

- scintillator crystals

pdg.lbl.gov

wavelength of maximum emission

Parameter:	ρ	MP	X_0*	R_M*	dE/dx* (for MIP)	λ_I*	τ_{decay}	λ_{max}	$n^\dagger$	Relative output‡	Hygro-scopic?	$d(LY)/dT$
Units:	g/cm^3	°C	cm	cm	MeV/cm	cm	ns	nm				%/°C§
NaI(Tl)	3.67	651	2.59	4.13	4.8	42.9	245	410	1.85	100	yes	−0.2
BGO	7.13	1050	1.12	2.23	9.0	22.8	300	480	2.15	21	no	−0.9
BaF_2	4.89	1280	2.03	3.10	6.5	30.7	650^s $<0.6^f$	300^s 220^f	1.50	36^s 4.1^f	no	-1.9^s 0.1^f
CsI(Tl)	4.51	621	1.86	3.57	5.6	39.3	1220	550	1.79	165	slight	0.4
CsI(Na)	4.51	621	1.86	3.57	5.6	39.3	690	420	1.84	88	yes	0.4
CsI(pure)	4.51	621	1.86	3.57	5.6	39.3	30^s 6^f	310	1.95	3.6^s 1.1^f	slight	−1.4
$PbWO_4$	8.30	1123	0.89	2.00	10.1	20.7	30^s 10^f	425^s 420^f	2.20	0.3^s 0.077^f	no	−2.5
LSO(Ce)	7.40	2050	1.14	2.07	9.6	20.9	40	402	1.82	85	no	−0.2
PbF_2	7.77	824	0.93	2.21	9.4	21.0	-	-	-	Cherenkov	no	-
CeF_3	6.16	1460	1.70	2.41	8.42	23.2	30	340	1.62	7.3	no	0
$LaBr_3$(Ce)	5.29	783	1.88	2.85	6.90	30.4	20	356	1.9	180	yes	0.2
$CeBr_3$	5.23	722	1.96	2.97	6.65	31.5	17	371	1.9	165	yes	−0.1

sensitive to humidity?

*Numerical values calculated using formulae in this review.
†Refractive index at the wavelength of the emission maximum.
‡Relative light output measured for samples of 1.5 X_0 cube with a Tyvek paper wrapping and a full end face coupled to a photodetector. The quantum efficiencies of the photodetector are taken out.
§Variation of light yield with temperature evaluated at the room temperature.
f = fast component, s = slow component

Light yield given relative to NaI(Tl) readout with PM (bialkali PC)

- Cerenkov radiators

Material	Density [g/cm^3]	X_0 [cm]	n	Light yield [p.e./GeV] (rel. p.e.)	λ_{cut} [nm]	Rad. Dam. [Gy]	Comments
SF-5 Lead glass	4.08	2.54	1.67	600 (1.5×10^{-4})	350	10^2	
SF-6 Lead glass	5.20	1.69	1.81	900 (2.3×10^{-4})	350	10^2	
PbF_2	7.66	0.95	1.82	2000 (5×10^{-4})		10^3	Not available in quantity

Cerenkov radiation

Cerenkov radiation emitted when a charged particle passes a medium with velocity $v \geq v_{light}$ in that medium

$$\beta \geq \beta_{thr} = \frac{1}{n} \quad n: \text{refractive index}$$

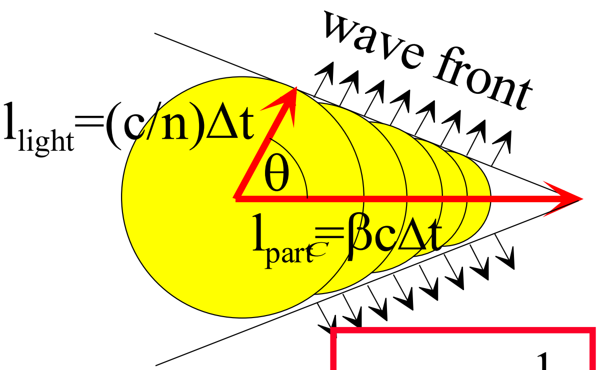

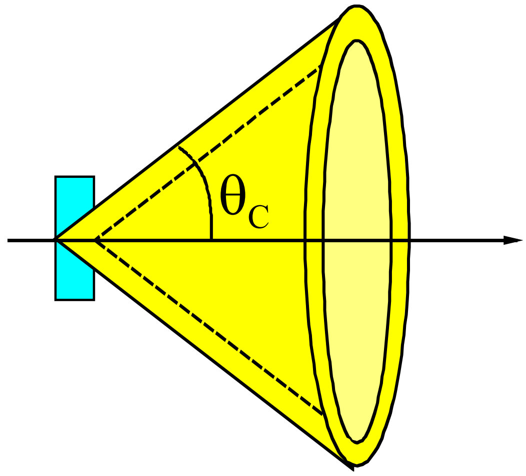

$$\boxed{\cos\theta_C = \frac{1}{n\beta}} \quad \text{with} \quad \underline{n = n(\lambda) \geq 1}$$

Cerenkov radiation emitted since particle polarizes atoms along its trajectory. If v > c/n this polarization not symmetric and there's a non-vanishing dipole field → emission of radiation

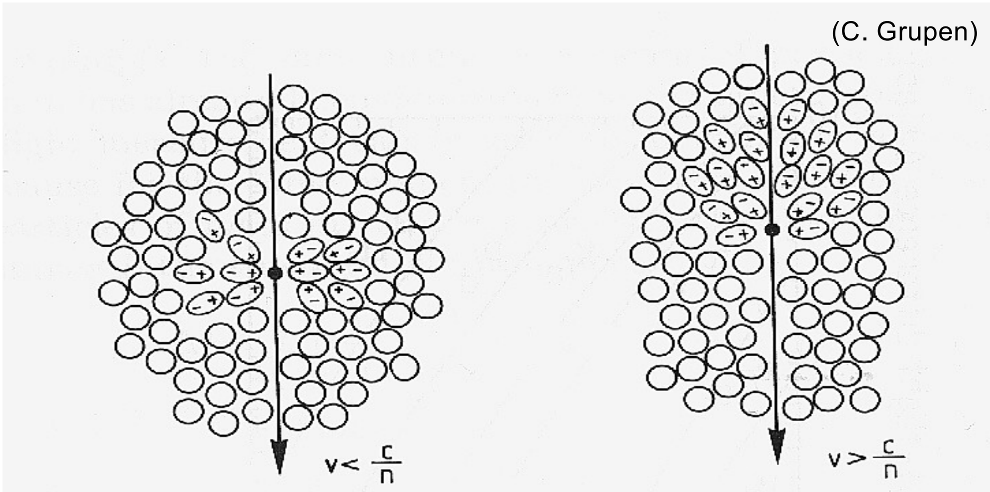

Fig. 6.7. Illustration of the Cherenkov effect [68].

OPAL Barrel + end-cap: lead glass + pre-sampler

(OPAL collab. NIM A 305 (1991) 275)

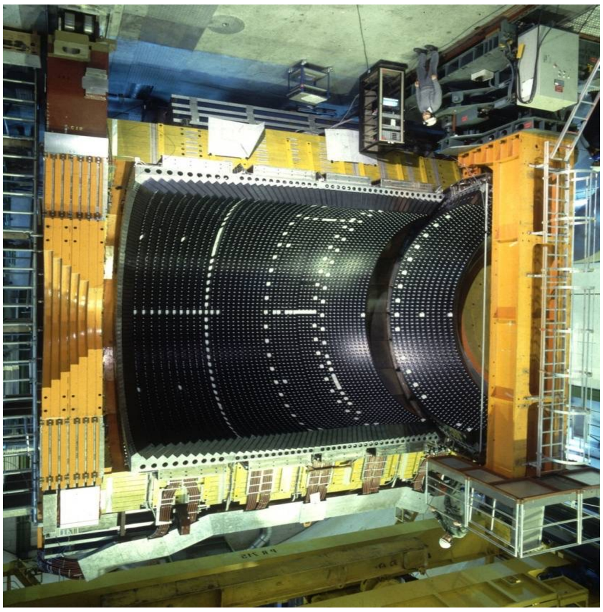

≈10,500 blocks (10 x 10 x 37 cm^3, 24.6 X_0), photo multiplier (barrel) or photo triode (end-cap) readout.

$$\frac{\sigma_E}{E} = \frac{6\ \%}{\sqrt{E[GeV]}} \oplus 0.2\ \%$$

Spatial resolution (intrinsic) ≈ 11 mm at 6 GeV

ECAL @ CMS

Precision electromagnetic calorimetry: 75848 PWO crystals

PWO: $PbWO_4$
about 10 m^3, 90 ton

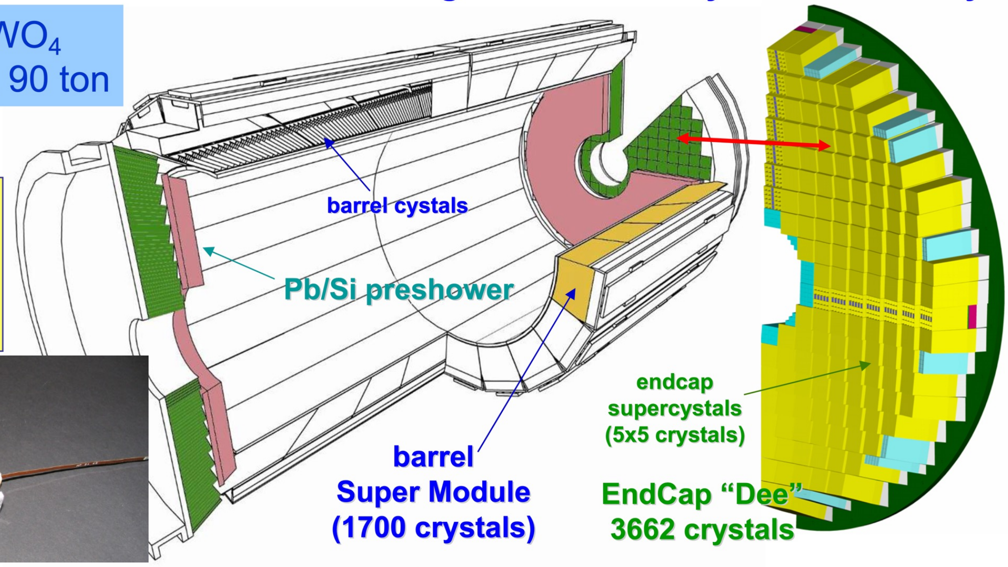

Previous Crystal calorimeters: max 1m^3

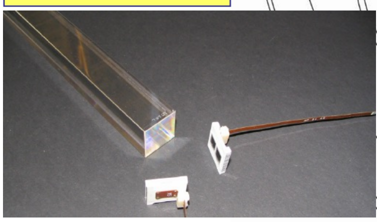

Barrel: $|\eta| < 1.48$
36 Super Modules
61200 crystals (2x2x23cm^3)

EndCaps: $1.48 < |\eta| < 3.0$
4 Dees
14648 crystals (3x3x22cm^3)

$$\sigma_E/E = 2.8\ \%/\sqrt{E[GeV]} \oplus 12\ \%/E[GeV] \oplus 0.3\ \%$$

Sampling calorimeters

absorber + detector separated $\rightarrow$ additional sampling fluctuations

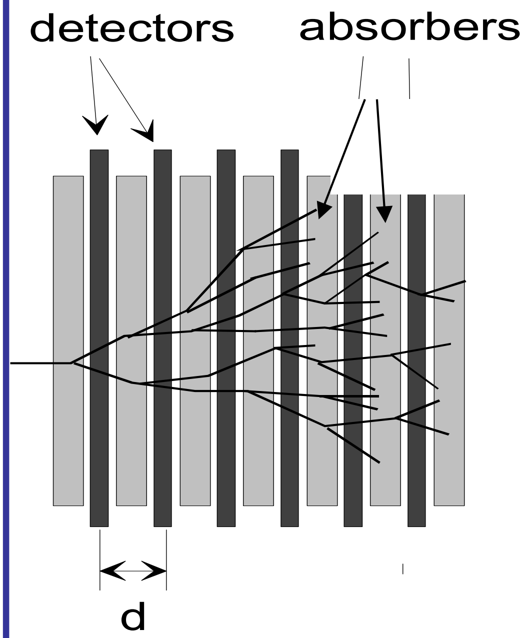

detectable track segments:

$$N = \frac{T_{det}}{d} \propto \frac{E}{E_c} X_0 \frac{1}{d}$$

"gain" factor

$$\frac{\sigma_E}{E} \propto \frac{\sqrt{N}}{N} \propto \sqrt{1/E} \cdot \sqrt{d/X_0}$$

- MWPC, streamer tubes
- warm liquids
  TMP = tetramethylpentane,
  TMS = tetramethylsilane
- cryogenic noble gases:
  mainly LAr (LXe, LKr)
- scintillators, scintillation fibers, silicon detectors

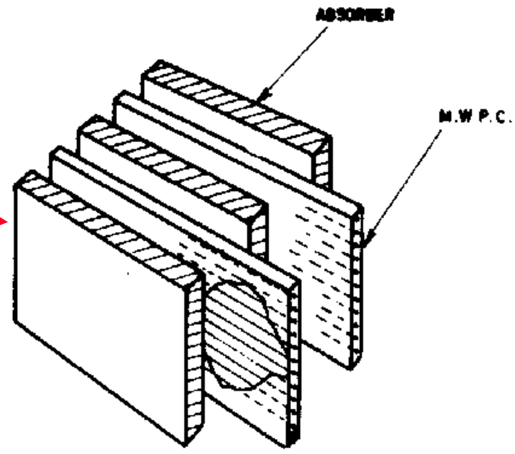

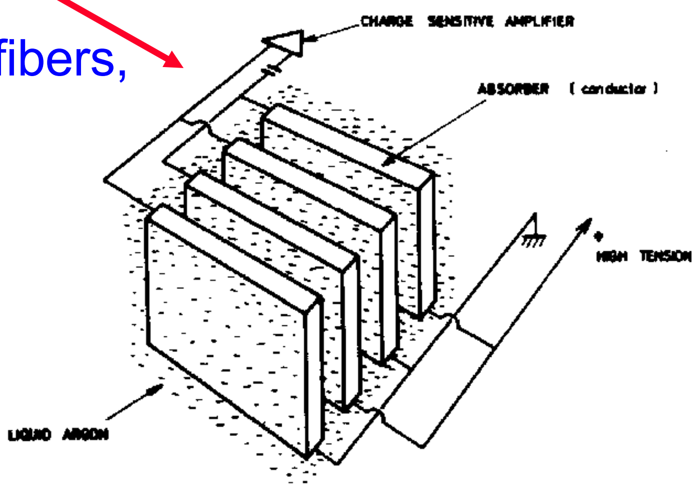

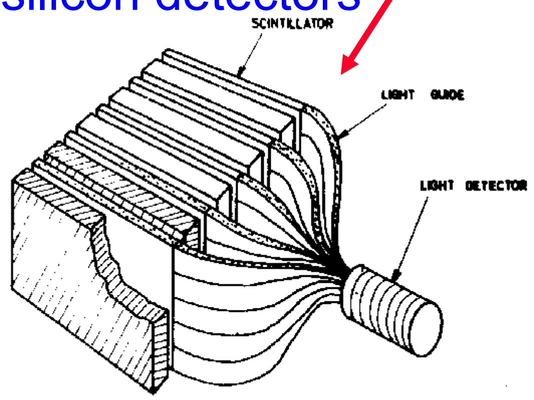

◆ ATLAS electromagnetic calorimeter

"accordion" geometry absorbers immersed in liquid argon

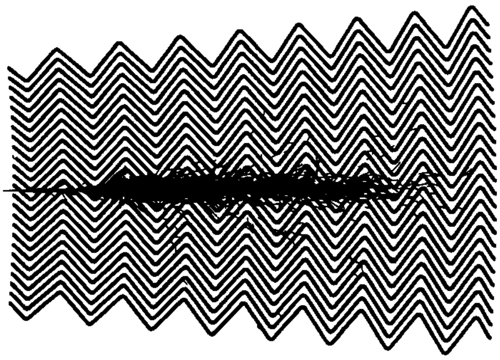

(RD3 / ATLAS)

Liquid Argon (90K)

+ lead-steal absorbers (1-2 mm)

+ multilayer copper-polyamide readout boards

→ ionization chamber.

1 GeV E-deposit → $5 \times 10^6\ e^-$

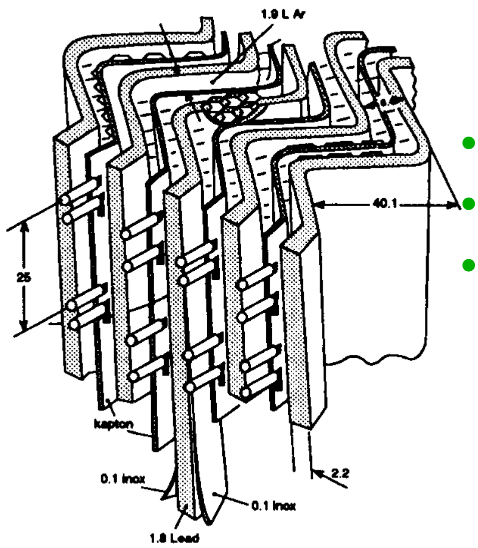

- geometry minimizes dead zones.
- liquid Ar intrinsically radiation hard.
- readout board allows fine segmentation (azimuth, pseudo-rapidity & longitudinal) according to physics needs

Test beam results, 300 GeV e^- (ATLAS TDR)

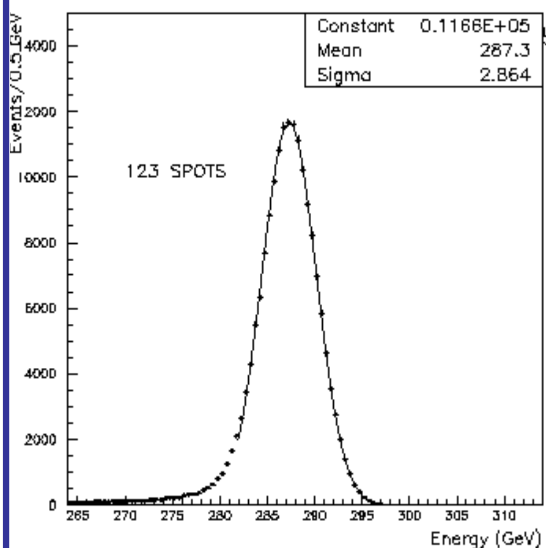

$$\frac{\sigma_E}{E} = \frac{a}{\sqrt{E}} \oplus \frac{b}{E} \oplus c$$

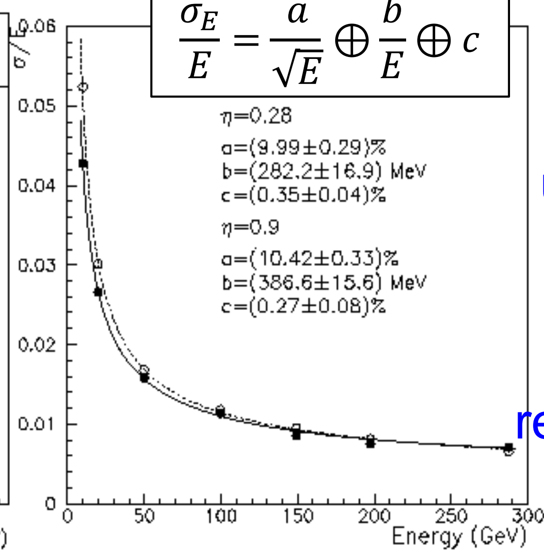

spatial & angular uniformity ≈ 0.5%

spatial resolution ≈ $5\ \text{mm}/\sqrt{E}$

◆ CMS hadron calorimeter

Brass (70 % Cu + 30 % Zn) absorber + scintillators

2 x 18 wedges (barrel) + 2 x 18 wedges (endcap)

in total: 1500 ton absorber

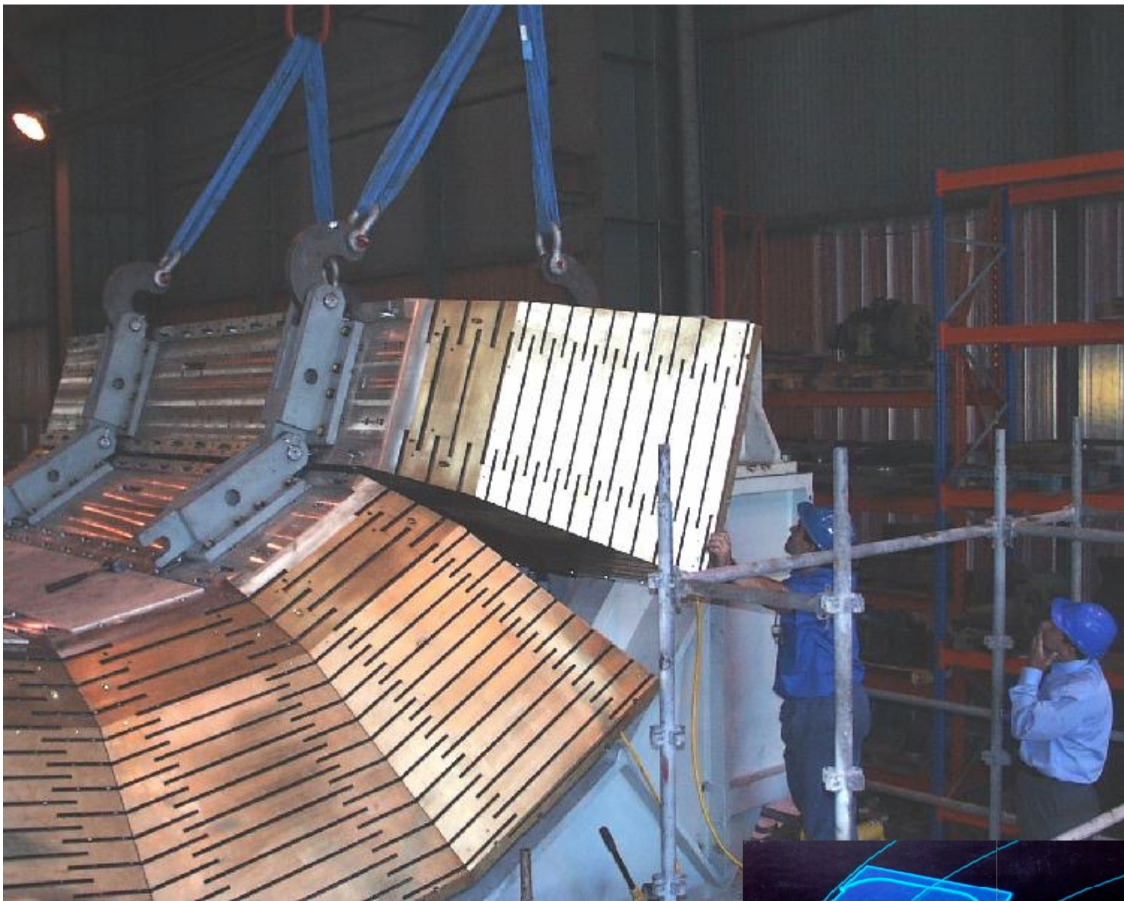

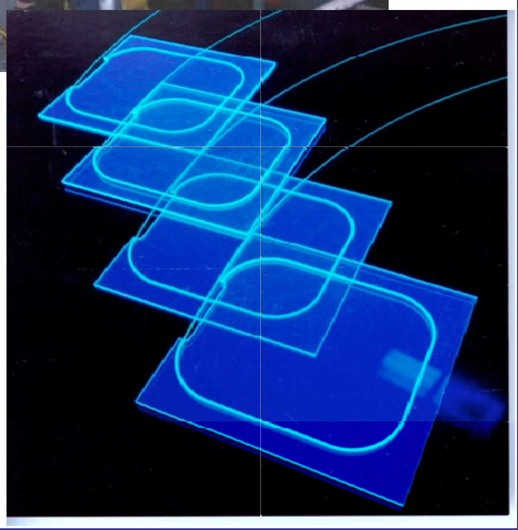

scintillators fill the slots &
read out done via fibres using
hybrid pixel detectors (HPDs)

energy resolution for single hadrons $\frac{\sigma_E}{E} = \frac{65\%}{\sqrt{E[GeV]}} \oplus 5\%$

Jet clustering

- Quarks/gluons not free particles (confinement) → fragment & hadronise into **jets** (bundles of nearby particles)
- Jets not uniquely defined → several algorithms (e.g. cone, k_T, anti-k_T, …) with several parameters that can be varied
- Ideally, $p_{\mathrm{jet}} = p_{q/g}$. In reality, correspondence not unique
- Most detectors get the direction quite precisely, but have more troubles with the energy (calorimeter response)

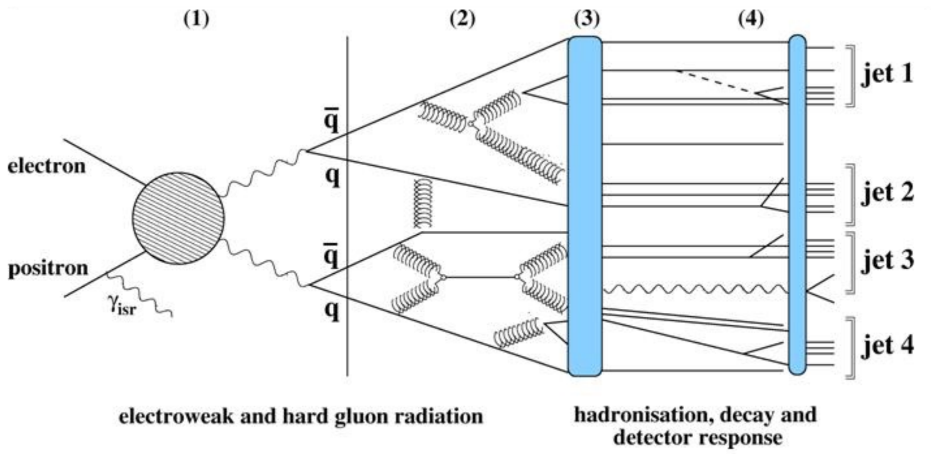

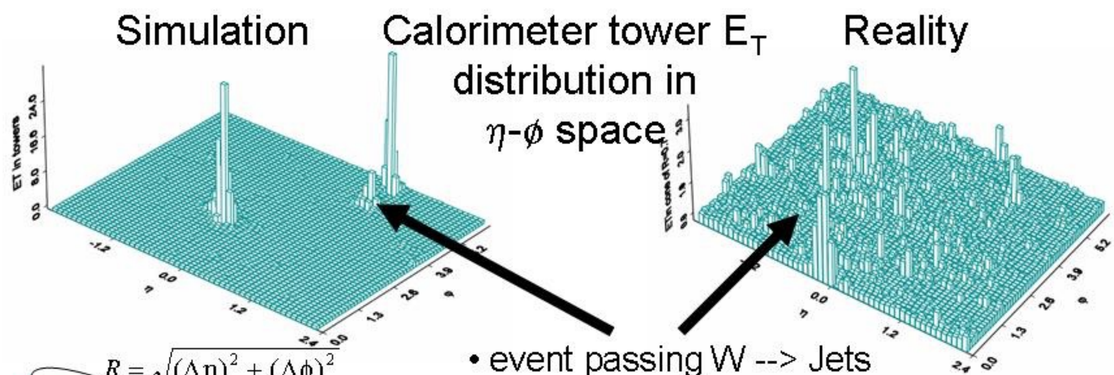

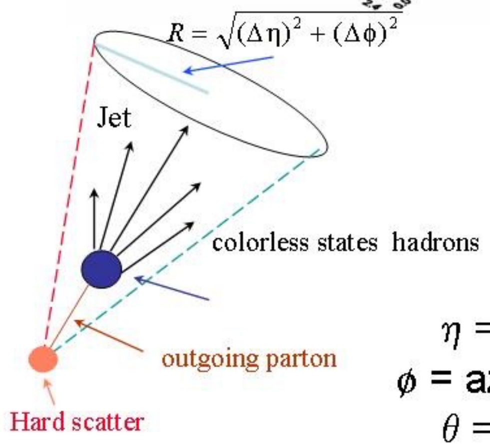

• event passing W --> Jets trigger: 2 central jets with E_T > 15 GeV
• high luminosity: several interactions per beam crossing + underlying event!
• dedicated clustering algorithms necessary: balance between theoretical correctness & simplicity: Cone Algorithm

$\eta = -\ln \tan(\theta/2)$
ϕ = azimuthal angle
θ = polar angle

At hadron colliders, jets formed using standardized jets algorithms like the cone algorithm (e.g. $R \approx 0.7$)

Measured jet p_T depends on the calorimeter response to hadrons

- generally non-linear (*absolute jet energy scale*)

Less energy in a jet:

- Particles deposit energy outside cone boundaries (*out-of-cone* and *splash-out)*

More energy in a jet:

- More than one beam particle interacts (*pileup*)
- Energy associated with the spectator partons (*underlying event, multi-parton interactions*)

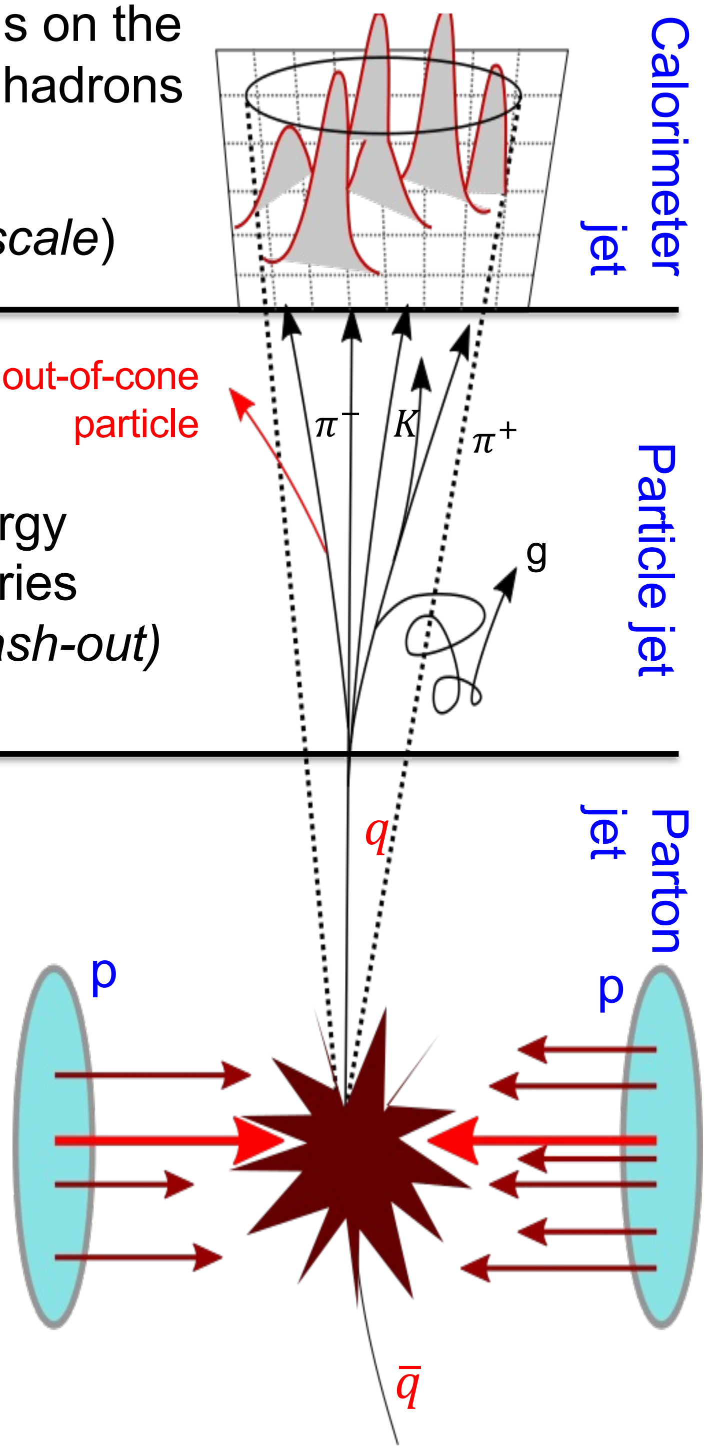

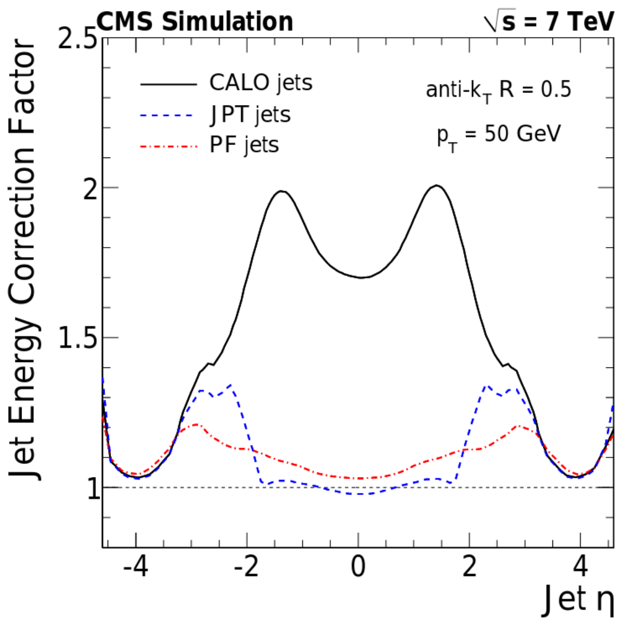

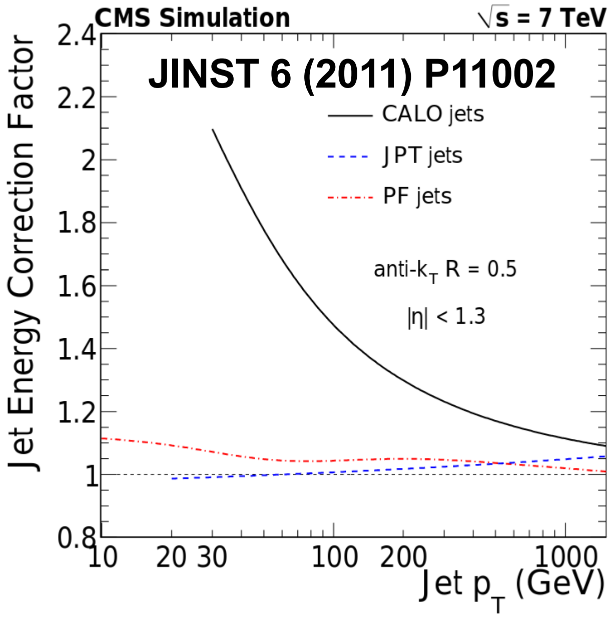

JPT & PF (CALO) = tracking+calorimetry (calorimetry only) jets

JPT = jet plus tracks; PF = particle flow, CHS = charged hadron subtraction

Corrections usually depend on jet kinematics (energy & direction(η, ϕ)) as well as jet flavour (gluon, light q, c or b)

Absolute energy calibration using well known & described processes like $Z^0 \to l^+ l^-$+ jet, γ+ jet, $W \to qq'$ whereas residual η-dependent corrections made using dijet events.

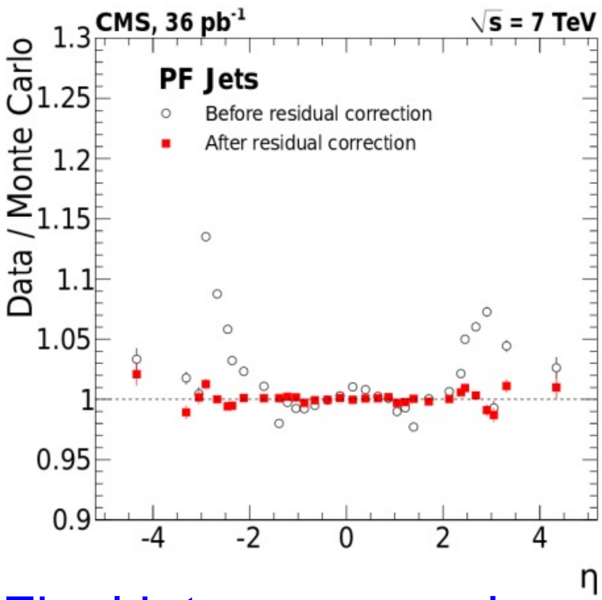

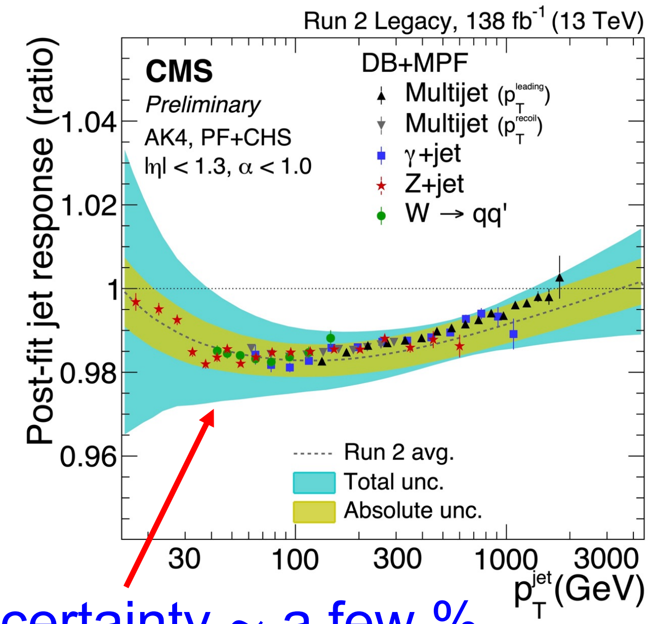

Final jet energy scale uncertainty ~ a few %

Constraint of missing energy through conservation of energy and momentum in detector

$$\overrightarrow{ME}_T = \vec{\not{E}}_T \equiv -\sum_i^{\text{objects}} \vec{p}_{T,i}$$

E.g. “detection” of invisible particles: ν’s, dark matter, …

Major “MET discoveries”: W boson ($W^\pm \to \ell\nu$), tau lepton ($e^+e^- \to e^\pm\mu^\mp 4\nu$), top quark ($t \to W^\pm b \to \ell\nu b$), …

Very sensitive to overall event definition:

- precise calibration of physics objects (leptons, γ’s, jets, …)
- track reconstruction (“spurious tracks”)
- pileup (additional pp interactions in same event)

Also profits from jet energy corrections:

$\sum \vec{p}_{T,ch}$ for each PU vertex

$$\begin{aligned}\overrightarrow{ME}_T^{corr} &= \overrightarrow{ME}_T - \vec{\Delta}_{jets} - \vec{\Delta}_{PU} \\ &= \overrightarrow{ME}_T - \textstyle\sum_{jets\ i}(\vec{p}_{T,i}^{\,corr} - \vec{p}_{T,i}) - \sum_{PU} f(\vec{v})\vec{v}\end{aligned}$$

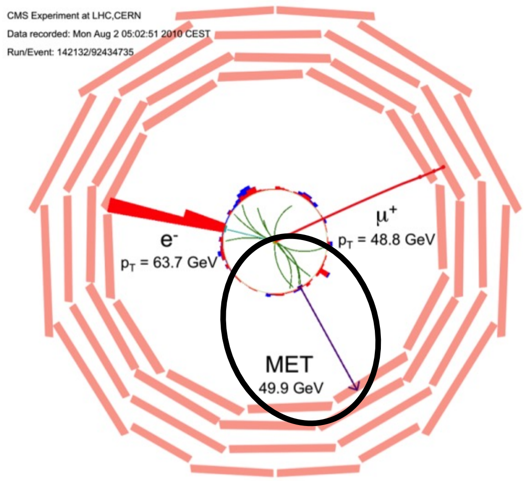

E.g. CMS $H \to W^+W^- \to \mu^+e^-\nu_\mu\,\bar{\nu}_e$ candidate (here, very low pileup (PU), $\langle n \rangle = 1.08$)

Particle flow

Goal: reconstruct all stable particles in an event (γ's, $h^{\pm}$, $\ell^{\pm}$)

Combining several fundamental ingredients from all subdetectors available:

- calorimeter clustering
- inner tracking, + extrapolation to the calorimeters
- leptons identification

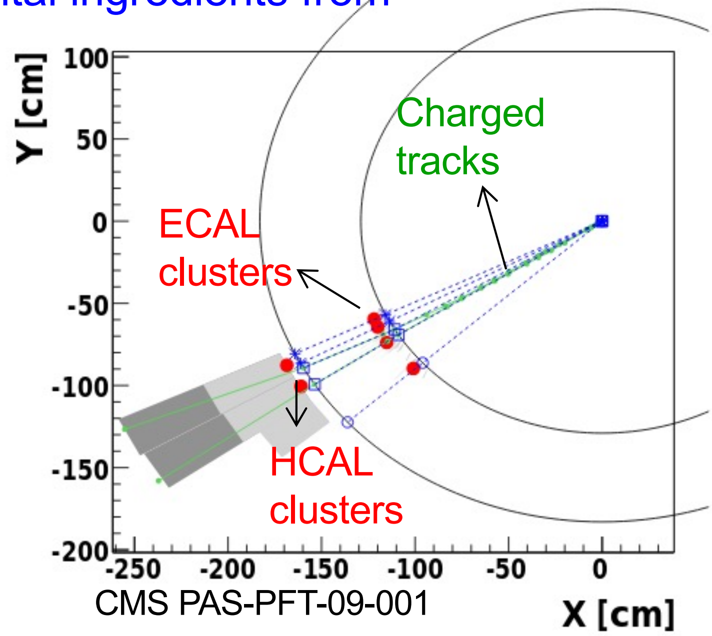

Linking topologically connected elements into "blocks" → particle flow candidates

Use candidates to reconstruct higher-level objects (MET, jets, τ leptons, isolated leptons, …) → particle identification

Algorithm: p from track, E from linked ECAL/HCAL cluster

- $E < p + \sigma_{\mathrm{calo}}$: add charged hadron only (except if identified μ)
- $E > p + \sigma_{\mathrm{calo}}$: add charged (according to p) & neutral hadron(s) (or π^0's, γ's) according to ECAL/HCAL energy deposits that exceeds p.

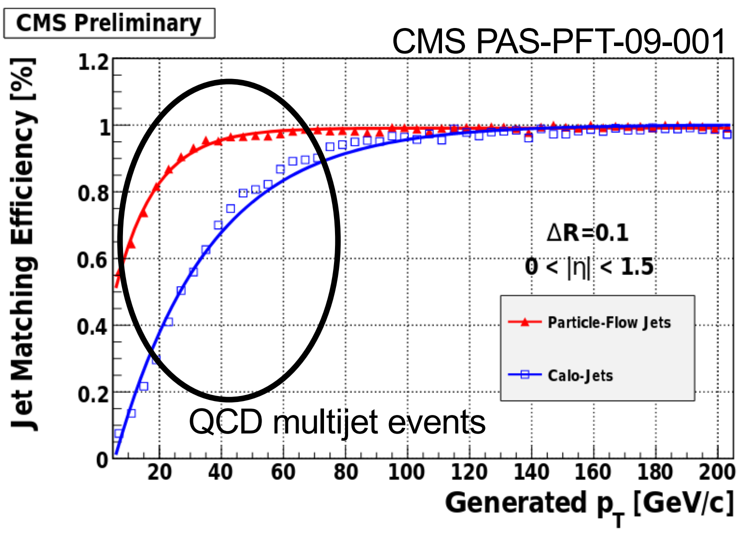

Energy of charged particles (→ jet energy) are measured more accurately with tracker than with calorimeter!